ELSEVIER

Biochimica et Biophysica Acta 1459 (2000) 10–34

BIOCHIMICA ET BIOPHYSICA ACTA
BBA

www.elsevier.com/locate/bba

# Reduction and protonation of the secondary quinone acceptor of *Rhodobacter sphaeroides* photosynthetic reaction center: kinetic model based on a comparison of wild-type chromatophores with mutants carrying Arg→Ile substitution at sites 207 and 217 in the L-subunit

Dmitry A. Cherepanov [a], Sergei I. Bibikov [b,c], Marina V. Bibikova [d], Dmitry A. Bloch [b], Lel A. Drachev [b], Oksana A. Gopta [b], Dieter Oesterhelt [c], Alexey Y. Semenov [b], Armen Y. Mulkidjanian [b,e,*]

[a] *Institute of Electrochemistry, Russian Academy of Sciences, Leninskii prosp. 31, 117071 Moscow, Russia*
[b] *A.N. Belozersky Institute of Physico-Chemical Biology, Moscow State University, 119899 Moscow, Russia*
[c] *Max-Plank-Institute für Biochimie, D-81152 Martinsried bei München, Germany*
[d] *N.I. Vavilov Institute of General Genetics, Russian Academy of Sciences, 117809 Moscow, Russia*
[e] *Abteilung Biophysik, Fachbereich Biologie/Chemie, Universität Osnabrück, D-49069 Osnabrück, Germany*

Received 23 April 1999; received in revised form 5 January 2000; accepted 21 February 2000

**Abstract**

After the light-induced charge separation in the photosynthetic reaction center (RC) of *Rhodobacter sphaeroides*, the electron reaches, via the tightly bound ubiquinone $Q_A$, the loosely bound ubiquinone $Q_B$. After two subsequent flashes of light, $Q_B$ is reduced to ubiquinol $Q_BH_2$, with a semiquinone anion $Q_B^-$ formed as an intermediate after the first flash. We studied $Q_BH_2$ formation in chromatophores from *Rb. sphaeroides* mutants that carried Arg→Ile substitution at sites 207 and 217 in the L-subunit. While Arg-L207 is 17 Å away from $Q_B$, Arg-L217 is closer (9 Å) and contacts the $Q_B$-binding pocket. From the pH dependence of the charge recombination in the RC after the first flash, we estimated $\Delta G_{AB}$, the free energy difference between the $Q_A^-Q_B$ and $Q_AQ_B^-$ states, and $pK_{212}$, the apparent p$K$ of Glu-L212, a residue that is only 4 Å away from $Q_B$. As expected, the replacement of positively charged arginines by neutral isoleucines destabilized the $Q_B^-$ state in the L217RI mutant to a larger extent than in the L207RI one. Also as expected, $pK_{212}$ increased by ~0.4 pH units in the L207RI mutant. The value of $pK_{212}$ in the L217RI mutant decreased by 0.3 pH units, contrary to expectations. The rate of the $Q_A^-Q_B^-\rightarrow Q_AQ_BH_2$ transition upon the second flash, as monitored by electrometry via the accompanying changes in the

Abbreviations: BChl, bacteriochlorophyll; $\Delta G_{AB}$, free energy gap between $Q_A/Q_A^-$ and $Q_B/Q_B^-$ redox pairs; $\delta\Delta G_{AB}$, change in the free energy gap between $Q_A/Q_A^-$ and $Q_B/Q_B^-$ redox pairs caused by the amino acid substitutions; $\delta\phi$, change in the local electrostatic potential; $\Delta\psi$, transmembrane electric potential; $\varepsilon_{eff}$, effective dielectric permittivity (dielectric constant); $E_a$, activation energy; $\lambda$, reorganization energy; MB, methylene blue; pH*, local proton activity; $pK_{212}$, p$K$ value of Glu-L212 residue ; $\delta pK_{212}$, change in the $pK_{212}$ value; $P$, P870, primary electron donor of RC; Q, ubiquinone; $QH_2$, ubiquinol; $Q_A$, $Q_A^-$, oxidized and single reduced (semiquinone) forms of the primary quinone acceptor, respectively; $Q_B$, $Q_B^-$, $Q_BH^\bullet$, $Q_B^{2-}$, $Q_BH^-$ $Q_BH_2$, oxidized form, semiquinone anion, semiquinone radical, doubly reduced non-protonated form, doubly reduced partly protonated form, and doubly reduced and doubly protonated (quinol) forms of the secondary quinone acceptor, respectively; $r_{AB}$, distance between $Q_A$ and $Q_B$; RC, photosynthetic reaction center; TMPD, *N*,*N*,*N*′,*N*′-tetramethyl-*p*-phenylenediamine; WT, wild-type

* Corresponding author. Fax: +49-541-969-2870; E-mail: mulkidjanian@biologie.uni-osnabrueck.de


PII: S0005-2728(00)00110-9

membrane potential, was two times faster in the L207RI mutant than in the wild-type, but remained essentially unchanged in the L217RI mutant. To rationalize these findings, we developed and analyzed a kinetic model of the $Q_A^- Q_B^- \rightarrow Q_A Q_B H_2$ transition. The model properly described the available experimental data and provided a set of quantitative kinetic and thermodynamic parameters of the $Q_B$ turnover. The non-electrostatic, 'chemical' affinity of the $Q_B$ site to protons proved to be as important for the attracting protons from the bulk, as the appropriate electrostatic potential. The mutation-caused changes in the chemical proton affinity could be estimated from the difference between the experimentally established $pK_{212}$ shifts and the expected changes in the electrostatic potential at Glu-L212, calculable from the X-ray structure of the RC. Based on functional studies, structural data and kinetic modeling, we suggest a mechanistic scheme of the $Q_B$ turnover. The detachment of the formed ubiquinol from its proximal position next to Glu-L212 is considered as the rate-limiting step of the reaction cycle. 

*Keywords:* Protein electrostatics; Photosynthetic reaction center; Ubiquinone; Electron transfer; Proton transfer; Electrogenesis; Membrane potential; *Rhodopseudomonas viridis*; *Rhodobacter sphaeroides*

## 1. Introduction

The photosynthetic reaction center (RC) of purple photosynthetic bacteria is a membrane pigment–protein complex that utilizes light energy to reduce a ubiquinone molecule (Q) to ubiquinol ($QH_2$). The RC is formed by two integral membrane subunits L and M which are capped by the H subunit from the cytoplasmic side of the membrane (see refs. [1,2] for the most recent crystal structures of *Rhodobacter sphaeroides* RC and ref. [3] for the general survey of the RC structures). Photoexcitation of RC causes a picosecond transmembrane electron transfer from the primary donor *P* (a bacteriochlorophyll dimer located between L and M subunits, closer to the periplasmic side of the chromatophore membrane), via bacteriopheophytin, to the quinone acceptors located at the cytoplasmic side of the RC (see ref. [4] for review). First the electron reaches, in ~200 ps, the primary quinone acceptor $Q_A$ that is tightly bound to the M subunit. Then the electron moves in ~100 μs to the loosely bound secondary quinone acceptor $Q_B$ located symmetrically at the L subunit. Fig. 1A shows $Q_B$ surrounded by some amino acid

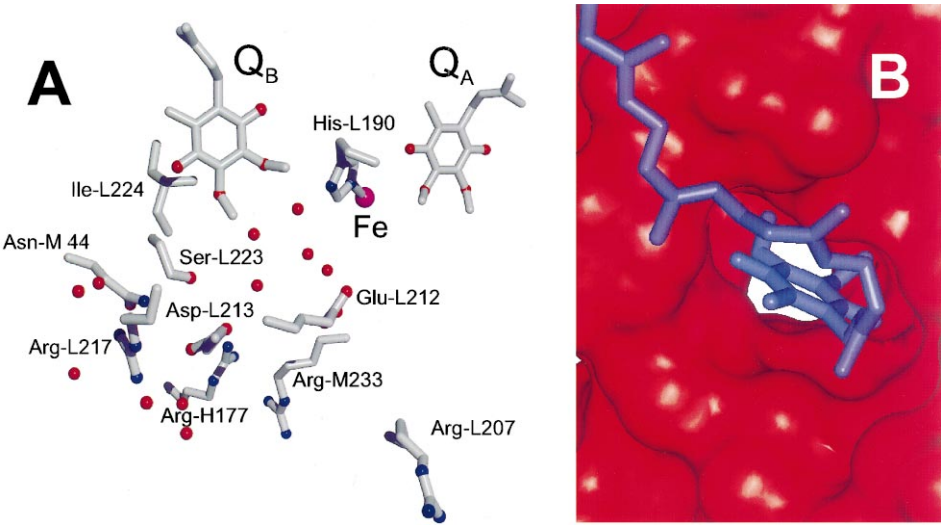


Fig. 1. Arrangement of the $Q_B$ site as inferred from the X-ray diffraction structure [1]. (A) Positions of the mutated and other relevant amino acid residues relative to $Q_B$ and to the non-heme iron are shown. Color code: oxygen, red; nitrogen, blue; hydrogen, where shown, yellow; iron, violet. (B) View on the $Q_B$ binding pocket from the intra-membrane flank of RC. The H subunit (located in the background) is not shown to emphasize the tunneling cavern in the structure. The surface was built by the Connolly algorithm [79] using the InsightII program (Molecular Simulations Inc.).

residues and water molecules (as obtained from the X-ray structure of the *Rb. sphaeroides* RC resolved at 2.2 Å [1]). The internal shape of the $Q_B$ binding cavity is shown in Fig. 1B. The $Q_B$ site looks like an opened cylinder or a tube where the ubiquinone molecule can move and even twist, pushing aside the loosely bound water molecules. The tube opens into a water-filled lens on the interface between the LM heterodimer and the H subunit. The direct connection between the water-filled lens and the $Q_B$-binding cavity allows both the effective intraprotein proton conduction and the fast exchange of ubiquinone with the membrane pool (see refs. [5–9] for reviews on $Q_B$ reduction and protonation in *Rb. sphaeroides*).

The delivery of the first electron to $Q_B$ causes the formation of a kinetically stable semiquinone anion radical $Q_B^{\bullet -}$ (hereafter denoted as $Q_B^-$ for simplicity):

$$Q_AQ_B \xrightarrow{1st\ h\nu} Q_A^{\bullet}Q_B \underset{l_-}{\overset{l_+}{\rightleftharpoons}} Q_AQ_B^{\bullet}$$

Scheme I.

While $Q_B$ can be easily exchanged for a ubiquinone from the membrane pool, $Q_B^-$ is tightly bound [10,11]. Although the semiquinone itself stays deprotonated, its negative charge shifts the p$K$ values of some amino acid residues in the vicinity and causes proton binding from the bulk both in the case of the isolated RC [12–14] and chromatophores [15]. The reaction (Scheme I) could be monitored either via electron transfer (see e.g. ref. [16]) or by monitoring the changes in the transmembrane electric potential ($\Delta\psi$) caused by proton transfer from the surface into the $Q_B$ site [15,17–21].

The delivery of the second electron leads to the ubiquinol formation that is coupled with proton uptake [12,13,15,22,23]:

$$Q_AQ_B^{\bullet} \xrightarrow{2nd\ h\nu} Q_A^{\bullet}Q_B^{\bullet} + 2H^+ \underset{m_-}{\overset{m_+}{\rightleftharpoons}} Q_AQ_BH_2 \ldots$$

$$\underset{k_{on}}{\overset{k_{off}}{\rightleftharpoons}} Q_A + QH_2$$

Scheme II.

This reaction could be traced by monitoring the electron transfer [15,24,25] or by measuring the electrogenesis of proton transfer through the membrane [15,17,18,21,26–28]. At room temperature (+25°C), the kinetics of the respective electrogenic reaction, B2, seem to be mono-exponential and could be characterized by a single rate constant, $k_{B2}$. Below +15°C, the B2 kinetics split into $B2_{fast}$ and $B2_{slow}$ components of similar amplitudes at neutral pH [28]. These two components, with differing activation energies $E_a$, have been attributed to the transfer of the first ($E_a \leq 10$ kJ/mol) and of the second ($E_a \sim 60$ kJ/mol) proton to $Q_B^-$ [28].

In this work, we characterized two mutants of *Rb. sphaeroides* with the positively charged residues around $Q_B$ replaced by the neutral ones (Arg-L207→Ile and Arg-L217→Ile). We attempted to complement the extensive studies of the negatively charged amino acid residues around $Q_B$ (see [7–9] for recent reviews). As expected, the replacement of the positively charged arginines by isoleucines decreased the stability of the $Q_AQ_B^-$ state in both mutants. At the same time, more complex perturbations in the electron/proton coupling during the $Q_A^-Q_B^- \rightarrow Q_AQ_BH_2$ transition could not be attributed to the electrostatic impact alone. Based on experimental data and kinetic modeling, we concluded that the non-electrostatic, 'chemical' affinity of the $Q_B$ site to protons is as important for their trapping from the bulk, as the electrostatic proton affinity that is due to the presence of a surplus negative charge. We suggest an approach that allows to estimate separately the impact of mutations on two types of proton affinity.

## 2. Materials and methods

### 2.1. Construction of mutants

Site-specific mutagenesis of the L subunit gene of the *Rb. sphaeroides* RC using the gapped-duplex method [29,30] was used to alter two basic amino acid residues located in the vicinity of the $Q_B$. Codons for arginine at positions 207 and 217 were each changed to those for isoleucine (L207RI and L217RI). Specifically, plasmid pMapLM1 of the pMac system [31], carrying the full and functionally active *pufQBALMX* operon and ampicillin resistance, was subjected to *Aat*II and *Pvu*II digestion to create a gap of 150 bp in the region of the L-sub-

unit gene. This plasmid was recombined with its single-stranded copy pMcpLM1 carrying chloramphenicol resistance. After addition of the appropriate oligonucleotide, the gap was filled-in with the Klenow fragment of DNA polymerase. The resulting plasmid was amplified in a *mutS* strain, and the mutated copy of the plasmid was selected after transformation of *Escherichia coli MV1190* on ampicillin plates and checked by sequencing using an ABI sequencer. The mutant copy of the *pufQBALMX* operon was moved to a mobilizable, broad host range plasmid pRK404, carrying tetracycline resistance [32,33] which was used to complement in trans the deletion strain *Rb. sphaeroides* Ga (Green neurosporene-accumulating variant) puf$\Delta$21/3 (*puf*$\Delta$*LMX*::kan ($Km^R$). The chromosomal copies of genes *pufQBA* were still active in this strain. The strain puf$\Delta$21/3, carrying the wild-type *pufQBALMX* operon in pRK404, was used as a control in most experiments and was designated as 'wild-type' (WT) in this paper. To avoid possible accumulation of revertants, mutant cells were routinely screened by sample sequencing.

### 2.2. Bacterial growth and preparation of chromatophores

*Rb. sphaeroides* mutants were grown semi-aerobically at 30°C in the dark of Sistrom's minimal medium supplemented with 0.2% (w/v) casamino acids, 25 μg/ml kanamycin and 2 μg/ml tetracycline, as described previously [34]. Cells were grown to late stationary phase in 1-l Erlenmeyer flasks, filled to 400 ml. Chromatophores were isolated by a ultrasonic disruption procedure (to decrease the cytochrome $c_2$ content) washed by ultracentrifugation and stored frozen in 150 mM sucrose at −20°C until used [28].

### 2.3. Photoexcitation source

Chromatophore samples were illuminated by single light pulses from a Q-switched neodymium YAG laser combined with a second harmonic generator (YG-481, Quantel, France, 532 nm, pulse half-width, 15 ns; 150 mJ/cm$^2$ per flash).

### 2.4. Differential spectroscopy

The kinetics of the laser flash-induced optical changes of $P$ were monitored at 603 nm using a home-built single-beam kinetical spectrophotometer with two monochromators interfaced to a DL-1080 (Datalab, UK) transient recorder and IBM-PC 486 computer. The pre-amplified transient signals were filtered through a low-frequency bandpass filter ($\tau$=10 μs), stored and averaged (usually, 10–20 curves) at 30-s dark intervals. The intensity of the permanent monitoring light beam was adjusted using the glass optical filters to keep $P$ 70–80% reduced. All measurements were carried out aerobically in 1×1×3 cm quartz cuvettes.

### 2.5. Electrometric measurements

The fast kinetics of the laser flash-induced membrane potential ($\Delta\psi$) generation in chromatophores were investigated by a direct electrometric technique [35]. The 0.2-μm-thick nitrocellulose film, that separated two Teflon compartments, was impregnated with a solution of soybean phosphatidylcholine (type II-S, Sigma, USA, 150 mg/ml) and coenzyme $Q_{10}$ (Sigma, USA, 20 mg/ml) in *n*-decane. Chromatophores (~80 μM bacteriochlorophyll *a*) were incubated in one of the compartments with 25 mM $CaCl_2$ for 3 h at 23°C, then the suspension was replaced by a buffer solution free of $CaCl_2$ and chromatophores. The voltage changes were monitored using Ag|AgCl electrodes, amplified by a high input impedance (~$10^{11}$ Ω) amplifier (3554BM, Burr-Brown, USA), and digitized by a DL1080 oscilloscope (Datalab, UK). The dwell time of the set-up was 100 ns. Chromatophores were pre-adapted in the complete darkness for 10–15 min before the applying series of light pulses, to achieve a full oxidation of the quinone acceptor complex by redox mediator methylene blue (MB). The concentration of the latter was determined experimentally for each pH region to achieve a full dark adaptation (see [10] for discussion of factors influencing the life time of $Q_B^-$). Then, a series of two flashes were applied with a 0.5-s dark interval between the flashes. To analyze the electrogenic phases attributed to the protonation of $Q_B$, the photoelectric responses obtained in the presence of a $Q_B$ site inhibitor stigmatellin were point-by-point subtracted from the first and second flash-induced photoelectric responses obtained without the inhibitor.

### 2.6. Calculations

The kinetic traces were analyzed by using the GIM software package developed by A.L. Drachev (Dr. Achev Development, USA). The DISCRETE algorithm [36] was used for the multi-exponential analysis of the optical and electrometric data. The kinetic models were analyzed numerically using the non-linear, non-gradient searching procedure known as Powell's algorithm [37].

## 3. Results

### 3.1. Charge recombination between $Q_B^-$ and $P^+$

In the absence of secondary electron donors, the charge separation between $P$ and quinone acceptors is followed by a charge recombination. At neutral pH, the recombination rate is slower when electron returns to $P^+$ from $Q_B^-$ ($\tau \sim 5$ s in chromatophores), than when it returns from $Q_A^-$ ($\tau \sim 100$ ms; the latter reaction is observed when the $Q_B$ site is blocked by inhibitor). Unlike those in the WT, the kinetics of charge recombination in the L207RI and L217RI mutants contained a fast component with a relative amplitude of $< 10\%$ and with a characteristic time of $P^+Q_A^-$ recombination (Fig. 2). This might be caused by the weaker ubiquinone binding to the $Q_B$ site in the mutants (see Section 4).

From the rate constant of electron return from $Q_A^-$ and $Q_B^-$, $k_{AP}$ and $k_{BP}$, the equilibrium constant $L$ of the electron distribution between $Q_A$ and $Q_B$ (see Scheme I) can be found by using the equation [38]:

$$L = k_{AP}/k_{BP} - 1 \quad (1)$$

The respective free energy difference could be calculated as

$$\Delta G_{AB} = -(2.3RT) \times lgL. \quad (2)$$

The pH dependence of $\Delta G_{AB}$ in the WT and mutant chromatophores is shown in the left panel of Fig. 3 (the slow component of $P^+Q_B^-$ recombination was used to calculate $\Delta G_{AB}$ in the case of mutants). The free energy gap between $Q_A^-Q_B$ and $Q_AQ_B^-$ states was smaller in both mutants than in the WT. The difference indicates that the $Q_AQ_B^-$ state was somewhat destabilized by the disappearance of the effective positive charges of Arg-L207 and Arg-L217.

The $P^+Q_B^- \rightarrow PQ_B$ recombination accelerated gradually on alkalinization, (see Fig. 2), whereas the rate of the $P^+Q_A^- \rightarrow PQ_A$ recombination, as measured in

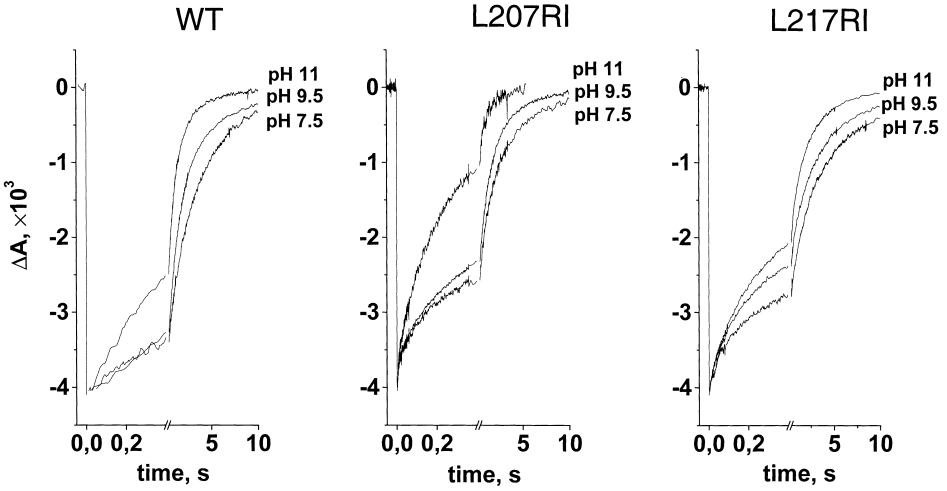


Fig. 2. Kinetics of the charge recombination reaction ($P^+Q_B^- \rightarrow PQ_B$) measured at 603 nm in the WT (left panel), L207RI (middle panel) and L217RI (right panel) chromatophores at various pH values, Conditions: 20 mM buffer (HEPES, CHES, or potassium phosphate), 50 mM KCl, 3 μM myxothiazole, 2 μM antimycin, 20 μg/ml gramicidin D. The concentration of BChl in the samples was 18 μM.

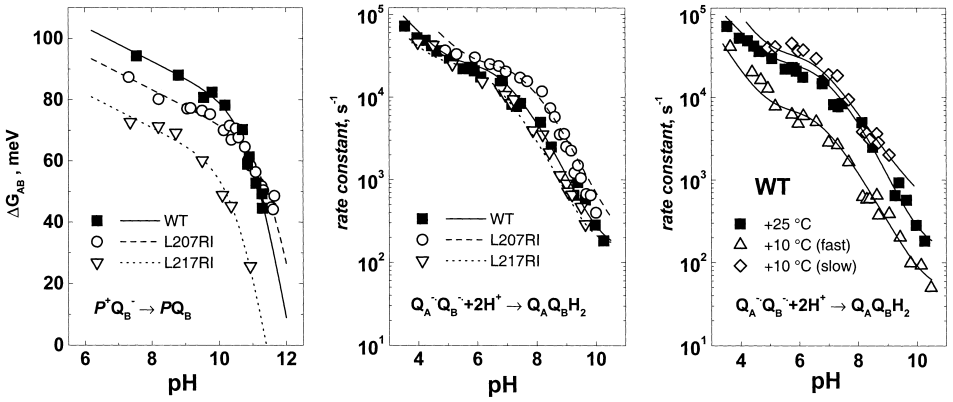


Fig. 3. pH dependence of the RC operation in chromatophores of *Rb. sphaeroides*: Left panel: pH dependence of the free energy difference $\Delta G_{AB}$ between $Q_A/Q_A^-$ and $Q_B/Q_B^-$ in WT (■); L207RI (○); L217RI (▽). Conditions as in Fig. 2, except 20 mM of one of the following buffers were present (MOPS, HEPES, Tris–HCl, CHES, CAPS, and potassium phosphate). The experimental points were fitted by using the set of parameters listed in Table 1 as is described in the text. Solid line, WT; dashed line, L207RI; dotted line, L217RI. Middle panel: pH dependence of the rate constant of B2 ($k_{B2}$) in WT (■); L207RI (○); L217RI (▽). See the caption to Fig. 5 for conditions. Right panel: pH dependence of the rate constant $k_{B2}$ in the WT chromatophores at +25°C (■), and of the rate constants of the B2 kinetic subcomponents $k_{B2\,fast}$ (◇) and $k_{B2\,slow}$ (△) at +10°C (data re-plotted from Fig. 3D in [28]). The theoretical curves in the middle and right panels were obtained by the global fit of the three data sets using the parameters listed in Table 1 (see the text for details).

the presence of a $Q_B$-antagonist stigmatellin, remained approximately constant (not shown). Correspondingly, the free energy gap between the $Q_A^-Q_B$ and $Q_AQ_B^-$ states, $\Delta G_{AB}$, decreased at higher pH, as it is shown in the left panel of Fig. 3. The pH dependence of $\Delta G_{AB}$ was weak at $6 < pH < 8$. Several amino acid residues that interact weakly with $Q_A^-$ and/or $Q_B^-$ have been proposed to account for this segment of pH dependence [5,6,13,14]). On further alkalinization, the pH dependence of $\Delta G_{AB}$ becomes stronger because of the destabilization of the $Q_AQ_B^-$ state by the negative charge that appears at Glu-L212 at pH above its apparent p$K$ (p$K_{212}$) of about 10.0. The absence of such a $Q_B^-$ destabilization in the L212EQ mutant [39,40] indicates that other amino acid residues contribute weakly in this pH range. Hence, we used the following phenomenological equation to describe the pH dependence of $\Delta G_{AB}$:

$$\Delta G_{AB} = \Delta G'_{AB} - 2.3RTlg\frac{1+10^{pH-pK_{212}-\Delta pK_{212}}}{1+10^{pH-pK_{212}}} - \chi\cdot 2.3RT(pH_i - pH), \quad (3)$$

where $\Delta G'_{AB}$ is the free energy difference at the isoelectric point ($pH_i$) that was estimated as 5.7 for chromatophores of *Rb. sphaeroides* [41]; p$K_{212}$ is p$K$ of Glu-L212 when $Q_B$ is neutral; $\Delta pK_{212}$ is the shift of p$K_{212}$ in response to the negative charge of $Q_B^-$; $\chi$ is an empirical coefficient that accounts for the weak, linear pH dependence of $\Delta G_{AB}$ at neutral pH. An estimate of ≥2.5 pH units from ref. [40] was used for $\Delta pK_{212}$. It was impossible to determine $\Delta pK_{212}$ from our data because the p$K$ value of Glu-L212 in

Table 1
Changes in $\Delta G_{AB}$ and in p$K_{212}$ in chromatophores of *Rb. sphaeroides* in response to the L207 Arg→Ile and L217 Arg→Ile substitutions (see text for details)

| Strain | $L_0$[a] | $\Delta G'_{AB}$ (meV) | $\delta G'_{AB}$ (meV) | p$K_{212}$ | $\delta pK_{212}$ |
|---|---|---|---|---|---|
| WT | 54 | −102.2 | 0 | 10.74 | 0 |
| L207RI | 40 | −94.7 | 7.5 | 11.17 | 0.43 |
| L217RI | 24 | −81.7 | 20.5 | 10.44 | −0.30 |

[a] $L_0$, equilibrium constant L at the isoelectric point (pH = 5.7).

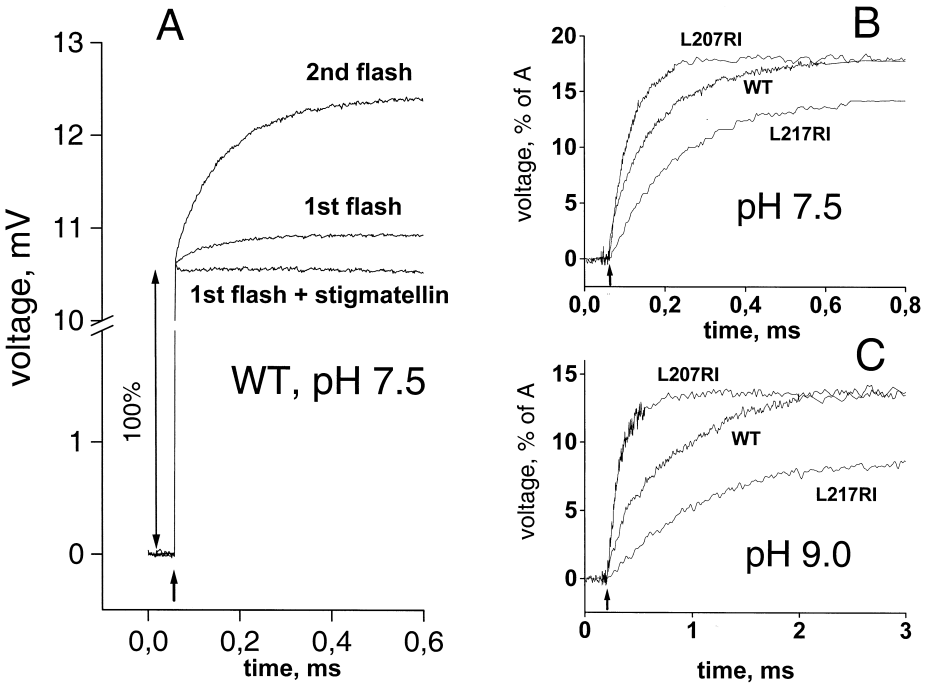


Fig. 4. Laser flash-induced voltage changes in the dark-adapted chromatophores. (A) The voltage transients upon the first and the second flash and upon the first flash in the presence of 1 μM stigmatellin. Conditions: 20 mM HEPES, pH 7.5, 50 mM KCl, 2 mM sodium ascorbate, 50 μM TMPD, 4 μM methylene blue, 4 μM myxothiazole, 2 μM antimycin A, +25°C. (B) The electrogenic phase B2 obtained as a difference between the 2nd flash-induced transient responses without an inhibitor and those in the presence of stigmatellin, pH 7.5. Conditions as in A, except 0.4 μM methylene blue was present in the case of L207RI. (C) The same as in Fig. 4B, but at pH 9.0. Conditions as in A except 20 mM CHES was present; MB was present at 2 μM (WT, L217RI) and 0.2 μM (L207RI), respectively. All traces were normalized to the amplitude of the A1 component (see text). Delay time between the first and second flashes, 0.5 s. The laser flashes are shown by arrows.

the presence of $Q_B^-$ was outside of the experimentally accessible pH range.

We used Eq. 3 to fit the experimental points, asking for the values of $\Delta G'_{AB}$ and p$K_{212}$ in the WT and the mutants. For simplicity, the slope coefficient $\chi$ was assumed to be the same for all three curves. The fit yielded a value of 0.093 for $\chi$; the obtained values of $\Delta G'_{AB}$ and p$K_{212}$ are presented in Table 1. The calculated theoretical curves are plotted in the left panel of Fig. 3.

Fig. 3 (left panel) and Table 1 show that the L217RI substitution caused a greater change in $\Delta G'_{AB}$ than the L207RI one. This is in agreement with the structure that shows Arg-L217 closer to $Q_B$ than Arg-L207 (Fig. 1A). Also in a rough accordance with the electrostatic theory, the deletion of a positive charge increased the p$K_{212}$ value of Glu-L212 by 0.4 pH units in the L207RI mutant (see Table 1). However, in the L217RI mutant p$K_{212}$ decreased by 0.3 pH units, contrary to the straightforward expectations based on electrostatics (see Section 4 for the further quantitative analysis).

### 3.2. Electrogenic reactions at the $Q_B$ site

Single-flash illumination of dark-adapted chromatophores of *Rb. sphaeroides* caused $\Delta\psi$ generation that was monitored electrometrically (Fig. 4). The initial fast $\Delta\psi$ formation (A1 and A2 components after the first and second flashes, respectively) was due to the transmembrane charge separation between *P* and $Q_A$ with a characteristic time $\tau < 100$ ns (see [42,43]). The charge separation was followed by the slower electrogenic component(s) ($\tau \sim 100$ μs at neutral pH) both after the first and the second flashes (Fig. 4A). To discriminate the charge displacements coupled with the $Q_B$ reduction, we applied stigmatel-

lin, a $Q_B$ antagonist [44][1]. It suppressed the slower components of the electrogenesis (see Fig. 4A).

### 3.2.1. The electrogenic reaction at the $Q_B$ site coupled with the $Q_B^-$ formation after the first flash

The electrogenic reaction at the $Q_B$ site coupled with the $Q_B^-$ formation after the first flash was discriminated as the difference between the first flash-induced photoelectric traces obtained in the absence and in the presence of stigmatellin, as established elsewhere [17]. The resulting component, B1, is likely to be caused by the electrogenic redistribution of charges in response to the $Q_B^-$ formation [17–19]. In the WT chromatophores, the extent of B1 increased at alkaline pH, reaching 5–7% of A1 at pH 9.5 (Fig. 5A). Concomitantly, the rate of B1 slowed down (Fig. 5B). Both effects are believed to reflect the protonation of Glu-L212 in response to $Q_B^-$ formation at $pH > pK_{212}$ [19,20,45]. As shown in Fig. 5A,B, in the L217RI mutant, the rate and the relative amplitude of B1 depended on pH, similarly to those in the WT chromatophores. With alkalinization, both the increase of the relative amplitude and the slowing of the rate were observed. In the L207RI mutant, the pattern was different: neither the increase in the relative amplitude of B1, nor the decrease of its rate were detectable up to pH 10.0.

### 3.2.2. The electrogenic reaction coupled with the $Q_BH_2$ formation after the second flash

The electrogenic reaction coupled with the $Q_BH_2$ formation after the second flash was discriminated as a difference of photoelectric responses induced by the second flash in the absence of the inhibitor and by the first flash in the presence of the latter (see Fig. 4B,C). The resulting electrogenic component, B2, reflects the transfer of two protons to $Q_B^-$ [15,17,26–28]. It is noteworthy that the amplitude of the initial charge separation after the second flash (component A2) was always smaller than those of the component A1 after the first one (by $\sim$2.5% at pH 7 in the WT). The difference was due to the presence of a small fraction of the RCs where the $Q_A^-Q_B$ state was thermally populated prior to the second flash. No stable charge separation was possible in this RC fraction. In the mutant chromatophores, the fraction was even larger, because the binding of $Q_B$ seemed to be impaired in some of the RC (see Section 4). Hence, the voltage transients measured after the second flash were routinely multiplied by the factor A1/A2 to normalize them to the first flash-induced kinetic traces (as was done, e.g. in Fig. 3).

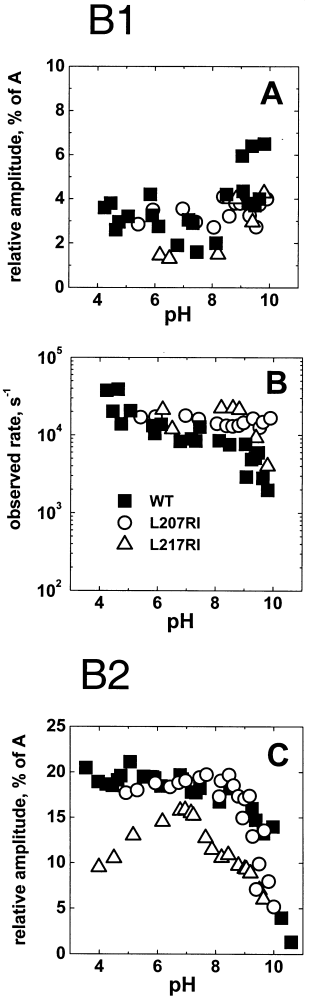


Fig. 5. pH dependence of the relative amplitude (A,C) and of the observed rate constant (B) of the electrogenic reaction at the $Q_B$ site upon the first (A,B) and the second (C) flashes. The amplitudes and the first-order rate constants ($k_{B1}$ and $k_{B2}$) of the electrogenic components B1 and B2 were obtained from the mono-exponential fits of data. ■, WT; ○, L207RI; ▽, L217RI. Conditions as in Fig. 4, except: (1) 20 mM of one of the following buffers were present (acetate, MES, MOPS, HEPES, Tris–HCl, CHES, CAPS, and potassium phosphate); and (2) the concentration of MB was varied in the range 0.1–16 μM, depending on pH.

[1] Similar results were obtained with atrazine and terbutryn, tested at random.

The pH dependence of the relative amplitude of B2 is presented in Fig. 5C. In the WT chromatophores, the relative extent of B2 was 15–20% of the phase A2 at pH < 9.0, and decreased at pH > 9.0, reflecting the decrease of the equilibrium constant of the $Q_A^- Q_B^- \rightarrow Q_A Q_B H_2$ reaction (see ref. [7,46]). As it follows from Figs. 4B,C and 5C, the relative amplitude of B2 phase was not affected by the mutation in the case of L207RI mutant, but was somewhat smaller in the L217RI mutant in the whole pH range.

The respective pH dependence of the rate constant of B2 is depicted not in Fig. 5, but in the middle panel of Fig. 3 (to make the further presentation of the modeling results more convenient). Three pH regions with differing slopes can be seen: two regions with a significant pH dependence (3.5 < pH < 5.5, and 8 < pH < 10), and a region with a weaker pH dependence (5.5 < pH < 8). This pattern was conserved in both mutants. As follows from Fig. 3 (middle panel), the rate of B2 was about two times faster in the L207RI mutant than in the WT in the whole pH range studied, but was almost similar to those in the WT in the case of the L217RI mutant.

## 4. Discussion

### 4.1. Binding of $Q_B$

In both mutants studied, the $P^+Q_B^-$ recombination kinetics included a small fast component with the characteristic time similar to those of the $P^+Q_A^-$ decay (see Fig. 2). It seems, that a small fraction of RC in those mutants lacked ubiquinone in the $Q_B$ site, in contrast to the WT where the site was fully occupied. Existence of a fraction of $Q_B$-lacking centers is also in line with lower A2/A1 ratio in the case of both mutants (not shown). Some distortion of the binding pocket also agrees with the observation that the oxidation of $Q_B^-$ by redox-mediators TMPD and MB was much faster in both mutants than in the WT (not shown).

### 4.2. $Q_A^- Q_B \rightarrow Q_A Q_B^-$ transition after the first flash

#### 4.2.1. Electrogenic component B1

At neutral pH, the electrogenicity of B1 is likely to be due to the redistribution of protons in response to the $Q_B^-$ formation [16,17,19,47,48]. At pH > p$K_{212}$, the $Q_B^-$ formation causes, in addition, the protonation of Glu-L212 from the bulk that leads to the overall increase of B1 and to its slowing [17–20]. The p$K_{212}$ value of ~9.5 attributable to Glu-L212 in chromatophores from electrometric data [17–19] resembles those obtained spectrophotometrically with the isolated RC (see refs. [20,39,40]), but is one pH unit lower than the estimates obtainable for chromatophores by ESR measurements [49] and by spectrophotometry (Fig. 3, left panel and Table 1). The difference might be explained by the quenching of the membrane surface potential by the residual $Ca^{2+}$ that may remain bound to the chromatophore membrane in the electrometric cell despite the washing (see Section 2). Another cause of the lower p$K_{212}$ might be the slightly detrimental influence of *n*-decane which was used to dissolve the phosphatidylcholine and ubiquinone (see Section 2).

In the L217RI mutant, the slowing of B1 was observed at pH > 9 (Fig. 5B). As in the WT, the slowing was accompanied by the increase in the relative amplitude of B1 (Fig. 5A). Both observations indicate that p$K_{212}$ was about 9–9.5 in the L217RI mutant. After correcting by one pH unit (see above), this estimate corresponds to the figure of 10.4 that was obtained from the kinetics of the charge recombination in this mutant (see Table 1). In the L207RI mutant, both the rate and the relative amplitude of B1 were pH independent up to pH 10. The p$K_{212}$ was estimated as 11.2 in the L207 mutant from the optical data (see Table 1). Taking into account the same correction of one pH unit, that is needed to compare the spectrophotometric and electrometric data (see above), an apparent p$K_{212}$ of ~10.2 could be expected for this mutant under the conditions of electrometric measurements. Unfortunately, we were unable to obtain reliable electrometric data at pH > 10 because of a sharp acceleration in the decay of the photoelectric response and the smaller extent of this response in the mutant chromatophores. Most likely, the electrogenic reactions of the Glu-L212 protonation in response to the $Q_B^-$ formation developed in the L207RI mutant at pH > 10, i.e. in the pH range which was inaccessible to our electrometric measurements.

*4.2.2. $P^+Q_AQ_B^- \rightarrow PQ_AQ_B$ charge recombination*

From the pH dependence of $P^+Q_B^- \rightarrow PQ_B$ recombination, we estimated $\Delta G'_{AB}$, the free energy gap of the $Q_A^-Q_B \leftrightarrow Q_AQ_B^-$ equilibrium at the isoelectric point ($pH_i$) of 5.7 (see Eq. 3), and $pK_{212}$ (see Table 1). In the case of the L207RI substitution, the free energy gap decreased by 8 meV compared to the WT. The distance between Arg-L207 and $Q_A$ ($r_A$) is 27 Å, whereas the distance between this residue and $Q_B$ ($r_B$) is 17 Å. The $\Delta G'_{AB}$ change could be attributed to the change in the electrostatic potential caused by the substitution. Then, using the Coulomb's equation

$$\delta\phi_{AB} = \frac{q}{\varepsilon_{eff}}\left(\frac{1}{r_B} - \frac{1}{r_A}\right), \quad (4)$$

where $\varepsilon_{eff}$ is the effective dielectric constant, and varying $r_A$ and $r_B$ in the range of ±1 Å (to allow for the limited resolution of the crystal structure), a $\varepsilon_{eff}$ estimate of 30÷45 could be obtained. It is noteworthy, that the application of Eq. 4 implies uniform $\varepsilon_{eff}$ between the L207 site and the $Q_A$ and $Q_B$ sites, respectively. This condition seems to hold in the case of the RC. The estimates of $\varepsilon_{eff}$ in the $Q_B$ site, which have been obtained previously from the influence of site-specific mutations at the site on the stability of $Q_B^-$, yielded values ranging between 20 and 48 [50–54]. On the other hand, the estimate of $\varepsilon_{eff}$, as could be obtained from the extent of Glu-L212 protonation in response to $Q_A^-$ formation, gives a comparable value of about 30 [55]. The particular reason of a rather homogenous and high $\varepsilon_{eff}$ may be the presence of a diffuse water cluster at the interface between the LM heterodimer and the H-subunit of RC. This cluster was resolved in the crystal structures [1,2,56–58]. It is expected to determine the dielectric properties in this part of the RC.

Similarly, the replacement of Arg-L217 by Ile is equivalent to the appearance of a negative charge some 10 Å away from $Q_B$ and 26 Å away from $Q_A$. Because Arg-L217 is closer to $Q_B$ than Arg-L207, its replacement causes stronger changes in $\Delta G'_{AB}$ (21 vs. 8 meV, see Table 1). The $\varepsilon_{eff}$ could be estimated as 35÷45.

The distance between the guanidinium group of Arg-L207 and the carboxy group of Glu-L212 side chain is ~12 Å. In the L207RI mutant, $pK_{212}$ increased by 0.43 pH units (see Table 1), in a rough agreement with an estimate that could be obtained by using the Coulomb's equation and by assuming $\varepsilon_{eff}$ of 30÷45. As Arg-L217 is also ~12 Å away from Glu-L212, the electrostatic impact of the L217RI substitution on $pK_{212}$ was expected to be of the same sign and amplitude as in the L207RI mutant. Instead, $pK_{212}$ in L217RI mutant was by 0.3 pH units lower than in the WT.

### *4.3. The $Q_A^-Q_B^- \rightarrow Q_AQ_BH_2$ transition after the second flash*

As seen in Figs. 4B,C and 5C, the relative extent of the electrogenic component B2 was smaller in the L217RI mutant than both in the L207RI one and in the WT. A plausible explanation might be a decreased amount of $Q_B^-$ before the second flash. The smaller $Q_B^-$ population could be due to the faster oxidation of $Q_B^-$ and/or $Q_A^-$ by the redox-mediator TMPD between the first and second flashes in the L217RI mutant (the respective bimolecular rate constant for the $Q_B^-$ oxidation was ≫10 times larger in the L217RI mutant than in the WT).

Unlike the $Q_A^-Q_B \rightarrow Q_AQ_B^-$ transition after the first flash that seems to be conformationally gated [59], the rate of the coupled transfer of the second electron and the first proton ($Q_A^-Q_B^- \rightarrow Q_AQ_BH^-$ transition) depends on $\Delta G_{AB}$ [60]. From the slope of this dependence, it has been concluded that the rate constant, $k_{AB}^{(2)}$, is proportional to the rate constant of the second electron transfer proper and to the fraction of the protonated $Q_B$ semiquinone [60], so that $k_{AB}^{(2)} = m_{+1} \times [Q_BH^\bullet]$. The replacement of charged amino acid residues could influence both factors. In the framework of the semiclassical Marcus theory [61], mutations could influence $m_{+1}$ via changes: (1) in the distance between $Q_A^-$ and $Q_B$, $r_{AB}$; (2) in the reorganization energy $\lambda$; and (3) in $\Delta G_{AB}$ (see ref. [61] and the Appendix). As one can see in the middle panel of Fig. 3, the rate constants of B2 almost coincided at pH < 5.0 in WT and two mutants. As the changes in $r_{AB}$ and in $\lambda$ are expected to be pH independent, we considered the convergence of the pH dependence curves at acidic pH as evidence against remarkable changes in $r_{AB}$ and in $\lambda$. Moreover, $Q_B^-$ is stabilized by several interactions with nearby amino acid residues, so that its ring is stretched between them (see structure C in Fig. 7 below). Even a minor,

mutation-caused displacement of $Q_B^-$ would cause a breakage of some of these bonds and lead to a destabilization of the $Q_AQ_B^-$ state. In the case of L207RI and L217RI mutants, even the inevitable electrostatic destabilization was minor (see Table 1).

On the other hand, the separation of the pH dependence curves at $pH > 5.0$ (Fig. 3, middle panel) indicated that the $[Q_BH^\bullet]$ extent was the one predominantly influenced by the mutations. Indeed, $k_{AB}^{(2)}$ is expected to be sensitive to the changes in $[Q_BH^\bullet]$ only above the p$K$ of the $Q_B^{\bullet-}/Q_BH^\bullet$ couple. This p$K$ has been shown to be about 5.0 in chromatophores of *Rb. sphaeroides* [21].

The replacement of the positively charged arginines by isoleucines was expected to cause a stronger impact on $[Q_BH^\bullet]$ than on $m_{+1}$. The $m_{+1}$ variations are determined by the changes in $\frac{1}{2}\delta\Delta G_{AB}$ that were minor (see Table 1 and Eqs. 14 and 15 in the Appendix), whereas the $[Q_BH^\bullet]$ amount is determined by the changes in the electrostatic potential at the $Q_B$ proper that were expected to be larger. To a first order, the disappearance of a positive charge was expected to accelerate the $Q_A^-Q_B^- \rightarrow Q_AQ_BH^-$ transition approximately three-fold in L207RI and six-fold in L217RI. The acceleration of B2 by a factor of two was indeed observed in the L207RI mutant (see Fig. 3, middle panel). In the case of L217RI, the rate of B2 was, however, almost unaffected by the mutation. The negligibly small impact of the L217RI substitution on the rate of the $Q_A^-Q_B^- \rightarrow Q_AQ_BH_2$ transition was rather peculiar, since Arg-L217 is located almost in the $Q_B$ binding pocket (see Fig. 1A). However, similarly small changes in the turnover rates compared with the WT have already been reported for the L217RL and L217RQ mutants [8]. As noted above, the L217RI mutation caused an acidic shift of p$K_{212}$ instead of an alkaline one that could be expected from electrostatic considerations. This p$K_{212}$ decrease indicated that the local effective concentration of protons (proton activity) in the $Q_B$ site decreased on the L217RI mutation, in spite of the deletion of a proton-repulsing positive charge. The proton activity at a protein site is determined not only by the electrostatic potential, but also by the non-electrostatic, 'chemical' affinity of the site to protons, particularly, by the amount and the state of proton-binding groups. The latter may change upon structural changes of protein thus influencing the proton transfer potential. The crystal structure [1] shows that Arg-L217, unlike Arg-L207, is in a direct contact with the $Q_B$-binding site and provides hydrogen bonds for two water molecules (they are depicted in Fig. 1A). It is plausible that the replacement of Arg-L217 by Ile might influence the chemical component of the local proton activity (by changing the time-averaged amount of water molecules in the $Q_B$ site and/or via a re-arrangement of the bound water) and thereby lead to the change in $[Q_BH^\bullet]$. To check whether the decrease in the chemical proton affinity could account for the observed similarity of B2 rates in the L217RI mutant and in the WT, we: (1) formalized the concept of the local proton activity; (2) estimated the factors that determine the local proton activity in the $Q_B$ site; and (3) developed and analyzed a kinetic model that couples the rate of the $Q_A^-Q_B^- \rightarrow Q_AQ_BH_2$ transition with the local proton activity at the $Q_B$ site.

### 4.4. Local proton activity (pH*) and its estimation in the $Q_B$ site

Quantitatively, the local proton activity in a protein cavity (e.g. in the $Q_B$-site), $[H^+]^*$, could be related to the proton concentration in the bulk, $[H^+]$, via: (1) the 'chemical' activity coefficient of proton $f$ that correlates the proton activity in the site to those in the bulk in the absence of the electrostatic field, so that $f = [H^+]^*/[H^+]$; and (2) the local electrostatic potential $\phi$:

$$[H^+]^* = f \cdot [H^+] \cdot 10^{-(\phi \cdot F)/(2.3RT)} \quad (5)$$

Correspondingly, the local pH (pH*) could be defined as:

$$pH^* = pH + \frac{\phi \cdot F}{2.3RT} + P \quad (6)$$

where $P = -\log(f)$ is the partitioning coefficient of proton.

As can be seen in the middle panel of Fig. 3, the rate constant of B2 depends strongly on pH at acidic and alkaline values, but is almost independent of pH at $6 < pH < 8$. The weak pH dependence at neutral pH has been reported previously for the $Q_A^-Q_B^- \rightarrow Q_AQ_BH_2$ transition when the latter has been monitored by electron transfer [12,25], proton uptake [22], and $\Delta\psi$ generation [17,18,41]. Under the

assumption that the rate of B2 was proportional to the proton activity at the surface, the weak pH dependence has been attributed to the influence of the surface electrostatic potential [41,62]. According to this kind of rationale, the number of negatively charged groups on the surface increases at alkaline pH, so that the concentration (activity) of protons at the surface increases relative to those in the bulk medium. As a result, any protolytic reaction at the surface is expected to be less pH dependent than the same reaction in the bulk solution[2]. The further studies have shown, however, that proton transfer into the $Q_B$ site from the surface does not limit the rate of the reaction [60]. This finding implies that the reaction rate depends on the proton activity in the $Q_B$ site, $pH^*_{Q_B}$, but not on the surface pH. $pH^*_{Q_B}$ would respond to the deprotonation of the ionizable groups both at the surface of the RC, that is only 5–15 Å away from the $Q_B$ site, and the $Q_B$ site proper. Under conditions similar to those in our study, the surface potential of *Rb. sphaeroides* chromatophores has been estimated to decrease from 0 mV at $pH_i$ of 5.7 down to −120 mV at pH of 10.0 [41]. In the simplest case, we can describe the pH dependence of $\phi_{surface}$ by a linear approximation:

$$\phi_{surface} = -\gamma \cdot (2.3RT/F) \cdot (pH - pH_i), \quad (7)$$

where $\gamma$ is an empirical coefficient of $0.3 \div 0.4$. By substituting this expression into Eq. 6, the linear relation between the surface and the bulk pH values can be obtained. A linear approximation of this kind could also account for the ionizable groups in the $Q_B$ site, if many of them interacted weakly with $Q_B$. This, however, is not the case. The electrostatic interaction of Glu-L212 with $Q_B$ has a magnitude of ~100 mV and is not weak [51]. We, however, can neglect the electrostatic impact of Glu-L212, as the latter is neutral in the presence of $Q_B^-$ at $pH < 12$. With a comparable strength $Q_B$ interacts also with an 'acidic cluster' that is contributed by Asp-L213, Asp-L210 and Asp-M17 [7,63,64]. The apparent p$K$ of the acidic cluster in the presence of $Q_B^-$, $pK_{acidic}$, is about 6.0 [20,40,49,65]. Above pH 6.0, the negative charge of the cluster decreases the electrostatic potential at $Q_B$ by ~100 mV [51].

To describe the electrostatic potential in the $Q_B$ site, $\phi_{Q_B}$, Eq. 7 is to be then modified as follows:

$$\phi_{Q_B} = -\gamma \cdot \frac{2.3RT}{F} \cdot (pH - pH_i) - \frac{\phi_{acidic}}{1 + 10^{pH - pK_{acidic}}}. \quad (8)$$

where $\phi_{acidic}$ is the electrostatic interaction of the acidic cluster with $Q_B$.

The validity of Eq. 8 follows from the studies of the RC with Asp-L213 replaced by Asn. The crystal structure of the RC stayed unchanged in this mutant compared to the WT [66]. However, the pH dependence of the second electron transfer became linear, with a steep slope of $0.6 \div 0.8$ in logarithmic coordinates (see refs. [40,65], the respective experimental points from ref. [65] are plotted in Fig. 6, right panel below). In this mutant, the rate of the second electron transfer has been shown to be limited by the proton uptake from the surface [67]. Correspondingly, the pH dependence of the rate constant followed the pH dependence of proton activity at the surface (Eq. 7) and not in the $Q_B$ site (Eq. 8).

Hence, the non-linear pH dependence of the rate constant of B2 (see Fig. 3, middle panel) seems to be contributed: (1) by a diffuse influence of weakly interacting ionizable groups leading to the decrease in the pH dependence slope from 1 to ~0.7 in the whole pH range; and (2) by a ~100 mV change in the local electrostatic potential in the $Q_B$ site due to a deprotonation event in the acidic cluster at $pH > 6.0$. This deprotonation causes a plateau in the pH dependence at $6.0 < pH < 8.0$.

#### 4.4.1. Summary

Summarizing this section, the $Q_B$ turnover rate depends on the local proton activity, pH*, in the immediate vicinity of $Q_B$ rather than on pH in the bulk or at the surface, as long as the proton delivery from the surface into the $Q_B$ is not the rate-limiting reaction [60]. According to Eq. 6, the pH* value is expected to be sensitive to the changes both in the local electrostatic field (via $\phi$) and in the local chemical proton affinity (via $P$). Correspondingly, we used $pH^*_{Q_B}$, as defined by Eqs. 6 and 8, instead of the bulk pH throughout the further modeling.

[2] A similar reasoning has been exploited independently to rationalize the non-linear pH dependence observed with bacteriorhodopsin [81].

### 4.5. Kinetic model of the $Q_A^- Q_B^- \rightarrow Q_A Q_B H_2$ transition

The question of how the changes in protein electrostatics could influence the rates of electron and proton transfer is of a general interest. Although the electro*static* calculations have been performed both for the RC of *Rb. sphaeroides* [63,64] and of *Rps. viridis* [68], their results could hardly be coupled with the *kinetics* of the respective electron and proton transfer reactions. The impossibility to calculate either pH* or its changes on mutations is among many obstacles. We used here an alternative approach and took the experimentally determined changes in $pK_{212}$ (see Table 1) as a measure of pH* changes in the $Q_B$ site in response to the mutations. Complementarily, the changes in $\Delta G_{AB}$ were utilized to estimate the dielectric properties of the $Q_B$ site. We inquired, to what extent the mutation-caused changes in the *rate* of the $Q_A^- Q_B^- \rightarrow Q_A Q_B H_2$ transition after the *second* flash are determined by the changes in the thermodynamic properties of the $Q_B$ site that are estimable from the charge recombination kinetics after the *first* flash.

The $Q_A^- Q_B^- \rightarrow Q_A Q_B H_2$ transition seems to be suitable for kinetic modeling. The reaction proceeds with both $Q_A^-$ and $Q_B^-$ tightly fixed in exact, known positions. The rate of the $Q_A^- Q_B^- \rightarrow Q_A Q_B H_2$ transition depends on the respective free energy difference [60] and, hence, is not limited by a conformational change. Therefore the impact of various factors (e.g. pH, ionic strength, amino acid substitutions) can be considered quantitatively. The kinetics of B2 were acceptably fitted by a single exponential at room temperature both in WT and both mutants (see Fig. 4B,C) that indicates the functional homogeneity of the $Q_B^-$-containing fraction of the RC. It is noteworthy, that the weaker $Q_B$ binding and the more pronounced interaction of $Q_B^-$ with redox-mediators in both mutants compared to the WT (see above) could influence the relative extent of B2, but not the rate of the $Q_A^- Q_B^- \rightarrow Q_A Q_B H_2$ transition that was modeled.

The reaction of $Q_B^-$ reduction could be described by the kinetic Scheme III (taken from ref. [7]) that is depicted below. Despite its complexity, the estimates for *all* the parameters are available. These estimates are presented in the upper row of Table 2 and substantiated in the Appendix.

Here indexes $m_{\pm 1}$, $m_{\pm 2}$ denote the direct/reverse rate constants of the second electron transfer reactions in two kinetic routes, respectively; $k_{\pm 1}$, $k_{\pm 2}$ are the rate constants of $Q_B$ protonation/deprotonation reactions involving the first proton ($H_I^+$) in two kinetic routes, respectively, $k_{\pm 3}$ denotes the direct/reverse rate constants of reactions involving the second proton ($H_{II}^+$); $k_{off}$, $k_{on}$ are the rate constants of the ubiquinol $Q_B H_2$ dissociation and binding in the site $Q_B$, respectively; $M_1$ is the equilibrium constant of the coupled transfer of the second electron and the first proton to $Q_B^-$; $M_2$ is the equilibrium constant of the $Q_B H_2$ formation; the equilibrium constant $M$ relates to the complete process of the reduction, protonation and dissociation of $Q_B H_2$ after the second flash.

#### 4.5.1. Mutation-caused changes in the rate of the second electron transfer

The mutation-caused changes in the rate of the

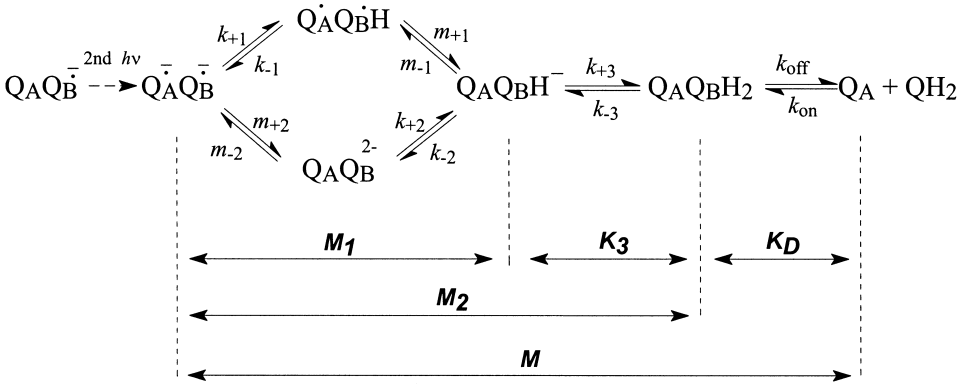


Scheme III.

second electron transfer, that owed to the changes in $\Delta G_{AB}$, could be calculated in the framework of the semiclassical Marcus theory [61] as is described in the Appendix.

#### 4.5.2. Mutation-caused changes in the local activity of protons

The mutation-caused changes in the local activity of protons, δpH*, were assumed, in accordance with Eq. 6, to be contributed by two terms, namely by the electrostatic influence of the mutation, $\delta\phi$, and by the change in the chemical proton partitioning coefficient, $\delta P$:

$$\delta\mathrm{pH}^* = \frac{\delta\phi \cdot F}{2.3RT} + \delta P \quad (9)$$

The electrostatic impact of mutations on $Q_B$ ($\delta\phi_{Q_B}$) was calculated by the Coulomb's equation,

$$\delta\phi_{Q_B} = \frac{1}{\varepsilon_{\mathrm{eff}} \times r_B},$$

where $r_B$, the distance between the substituted residue and $Q_B$ was taken from the crystal structure. The change in the partitioning coefficient $\delta P$ was assumed to be uniform throughout the $Q_B$-binding pocket and was estimated from the p$K$ shift of Glu-L212 residue:

$$\delta P = -\delta\mathrm{p}K_{212} - \frac{\delta\phi_{212} \cdot F}{2.3RT} \quad (10)$$

Here $\delta\phi_{212}$, the electrostatic impact of mutations on Glu-L212, was calculated by the Coulomb's equation as described above, with the only difference that the distance between the substituted residue and the carboxy group of Glu-L212 was taken on calculation. Eq. 10 implies that the experimentally determined p$K$ shifts of Glu-L212, $\delta\mathrm{p}K_{212}$, (see Table 1) reflected both the electrostatic impact of mutations on Glu-L212, that could be independently calculated from the crystal structure, and the changes in the chemical affinity to proton, $\delta P$. Correspondingly, the latter value could be estimated from the difference between the experimentally established p$K_{212}$ shifts (see Table 1) and the expected changes in the electrostatic potential at Glu-L212 calculable from the X-ray structure of the RC.

#### 4.5.3. Chromatophores of Rb. sphaeroides

Taking the kinetic and thermodynamic parameters as defined above and in the Appendix, we included them into a kinetic model that described the electron and proton transfer reactions at the $Q_B$ site upon the second flash in accordance with Scheme III. The respective system of differential equations and its mathematical solution are presented in the Appendix. The list of the independently varied parameters is given in Table 2.

Three data sets were modeled simultaneously:

1. the pH dependence of $\Delta G_{AB}$ as determined from the $P^+Q_AQ_B^- \rightarrow PQ_AQ_B$ charge recombination kinetics in the WT and L207RI and L217RI mutants (Fig. 3, left panel). We used these data to estimate the changes in $\Delta G_{AB}$ and in the non-electrostatic proton affinity ($\delta P$) (see Table 1 and Eqs. 9 and 10);
2. the pH dependence of the B2 rate constant ($Q_A^-Q_B^- \rightarrow Q_AQ_BH_2$ reaction) in the WT and L207RI and L217RI mutants at +25°C (Fig. 3, middle panel); and
3. the pH dependence of the rate constants of the slow and the fast components of B2 as resolved in the WT chromatophores at +10°C (Fig. 3, right panel). Originally published elsewhere [28], these data reflect the pH dependence of the rates of the first ($B2_{fast}$) and the second ($B2_{slow}$) proton transfer to $Q_B$. The correspondence of the model with these data seemed to be crucial for the reliability of the modeling.

Table 2
Parameters of the $Q_A^-Q_B^- \rightarrow Q_AQ_BH_2$ transition (see Scheme III) in chromatophores of *Rb. sphaeroides*

| Variable | $\gamma$ | p$K_{acidic}$ | $\phi_{acidic}$ (mV) | p$K_1$ | p$K_2$ | $m_{+1}$ ($s^{-1}$) | $m_{+2}$ ($s^{-1}$) | $k_{+3}$ ($s^{-1}$, pH 7) | p$K_3$ |
|---|---|---|---|---|---|---|---|---|---|
| Initial | 0.4 | 6.0 | 100 | 5.0 | 10.5 | $10^5$ | $10^3$ | $10^4$ | 10.5 |
| Final | 0.38 | 5.84 | 83 | 4.2 | >11 | $8.89 \cdot 10^4$ | $<10^3$ | $1.68 \cdot 10^4$ | 10.95 |

Top row: the initial, parameter set as obtained from the literature. Bottom row: the final parameter values as obtained by the optimization fit of experimental data in the middle and right panels of Fig. 3. See text for details.

Table 3
Mutation-caused changes in $\delta\phi_{Q_B}$, $\delta\phi_{212}$, and $\delta P$ in chromatophores and the isolated RC preparations of *Rb. sphaeroides*

| | Chromatophores | | Isolated reaction centers | | | |
|---|---|---|---|---|---|---|
| | L207RI | L217RI | L213DN | L213DN/M44ND | M44ND | L213DN/H177ND |
| $\delta\phi_{Q_B}$ | −23.8 mV | −54.0 mV | 63.5 mV | 2.9 mV | −60.6 mV | 34.5 mV |
| $\delta\phi_{212}$ | −31.5 mV | −34.7 mV | 55.6 mV | 19.5 mV | −36.0 mV | 23.3 mV |
| $\delta P$ | 0.10 | 0.89 | 0.27 | 0.25 | 0.0 | 0.49 |

See the text for the calculation procedure.

The obtained model curves described quantitatively the whole set of data (see the lines plotted in all panels of Fig. 3). The found parameter values (Table 2, bottom) were close to the initial estimates that were derived from the literature (Table 2, top). The model predicted both the acceleration of the reaction kinetics in the L207RI mutant and the small deviations from the WT rates in the L217RI mutant. Reasonable fits were obtained when the $\varepsilon_{eff}$ value was varied in the range $30 \div 40$. This range corresponds to the estimates of $\varepsilon_{eff}$ in the $Q_B$ site that were obtained from the functional data both by us and by others (see above). The best fit was obtained with $\varepsilon_{eff} = 36$. Table 3 shows values of $\delta\phi_{Q_B}$, $\delta\phi_{212}$, and $\delta P$ that correspond to $\varepsilon_{eff} = 36$. It is noteworthy, that no reasonable fit was possible unless the possibility of changes in the local, chemical affinity to proton was explicitly taken into account as described by Eq. 9. The modeling shows, that although the L217RI substitution caused a stronger change in the electrostatic potential in the $Q_B$ site compared to the L207RI (see Fig. 3, left panel and Table 3), the opposite impacts from the changes in the electrostatic and chemical proton affinities seemed to compensate each other, so that the kinetics of $Q_A^- Q_B^- \rightarrow Q_A Q_B H_2$ reaction in the L217RI mutant resembled those in the WT chromatophores (Fig. 3, middle panel).

#### 4.5.4. Isolated RC of Rb. sphaeroides

The presented model is directly applicable only to the RC mutants which retain the Glu-L212 residue, because the changes in $pK_{212}$ are used as a measure of the proton affinity changes in the $Q_B$ site. Another restriction is the absence of kinetic limitation by proton transfer. We assumed an absence of such a limitation in the studied two mutants because neither the proton-transferring acidic residues were replaced, nor the rate of the electrogenic proton transfer was slowed down (it even increased in the L207RI mutant). The assumption, still, may not hold for any arbitrary mutant. From the dependence of the second electron transfer rate $k_{AB}^{(2)}$ and $\Delta G_{AB}$, it has been recently concluded that proton transfer is not limiting, besides the WT, also in the M44ND, L213DN/M44ND, L213DN/H177RH and L213DN/M233RC mutants of *Rb. sphaeroides* [67]. So we put the model on a test and checked, whether it could predict the changes in the pH dependence of the second electron transfer rate in these mutants from the changes in the pH dependence of their $P^+Q_B^-$ recombination kinetics.

In Fig. 6 (both panels), the original experimental data from refs. [65,67,69] are plotted[3]. These pH dependence curves were obtained with isolated RC and differ somewhat from those in chromatophores. Therefore, we initially fitted the pH dependence curves of the $P^+Q_B^-$ recombination in the left panel of Fig. 6 to estimate the values of $\delta\Delta G'_{AB}$ and $\delta pK_{212}$ for the WT and mutant RC preparations. The same fitting procedure, as described for chromatophores in Section 3, was used. The obtained estimates are presented in Table 4.

In the case of the isolated RC, the rate constants not of B2, but of the second electron transfer, $k_{AB}^{(2)}$ ($Q_A^- Q_B^- \rightarrow Q_A Q_B H^-$ reaction), were available. Using the values from Table 4, we *calculated* the theoretical pH dependence of $k_{AB}^{(2)}$ in isolated RC as is described in the Appendix. The fixed $\varepsilon_{eff} = 36$ was taken on

[3] The pH dependence both of the $P^+Q_B^- \rightarrow PQ_B$ back reaction and of $k_{AB}^{(2)}$ were similar in L213DN/H177RH and L213DN/M233RC double mutants at $pH > 6.0$ [67], therefore, in Fig. 6, we only depicted the L213DN/H177RH data.

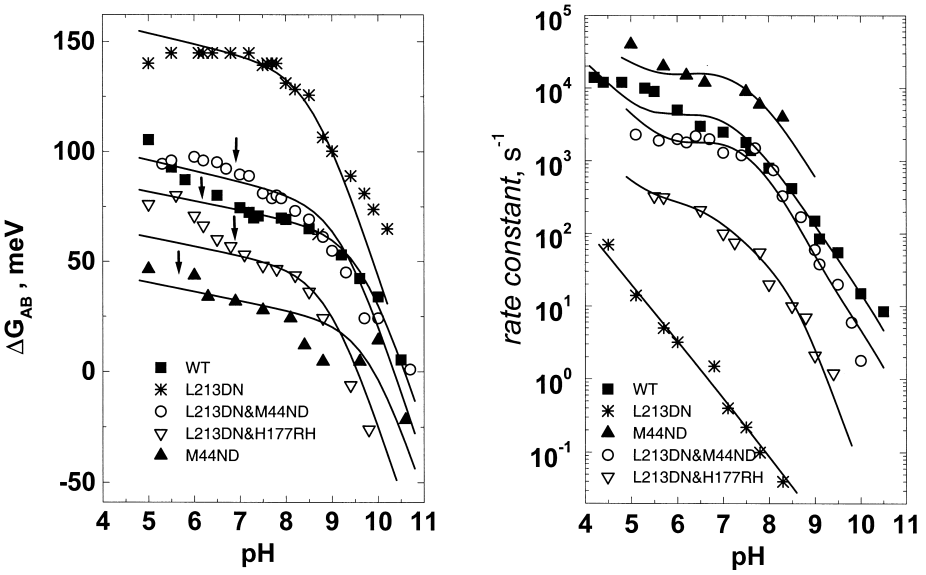


Fig. 6. pH dependence of the $Q_B$ turnover in the isolated RC of *Rb. sphaeroides*. Left panel: pH dependence of the first electron equilibrium constant between $Q_A^-Q_B$ and $Q_AQ_B^-$ states. Right panel: pH dependence of the rate constant of the second electron transfer reaction $k_{AB}^{(2)}$ (the original experimental data, published in [65,67,69] were kindly provided by M.Y. Okamura and M.L. Paddock). Theoretical curves were calculated as described in the text, the respective parameter values are listed in Tables 3–5.

calculations, for simplicity. The replacement of Asp-L213 by Asn in some mutants could cause changes in the composition and/or properties of the acidic cluster. To account for such changes, we treated $\phi_{acidic}$ and $pK_{acidic}$ as variable parameters upon the modeling of the RC data. The calculated curves are plotted in the right panel of Fig. 6, and the parameter values are summarized in Tables 3, 5 and 6.

Fig. 6 shows that the model straightforwardly predicted the changes in the pH dependence of $k_{AB}^{(2)}$, as compared to the WT, from the changes in the respective pH dependence of the $P^+Q_B^- \rightarrow PQ_B$ back reaction for *all the mutants*. It is noteworthy that the fit of the experimental points was achieved with parameter values that were very close both to the initial estimates (that were derived from the literature, see the upper line in Table 2) and to the chromatophore parameters (compare with the lower line in Table 2).

For comparison, the data on L213DN were also analyzed (see both panels of Fig. 6). Here, the pH dependence of the B2 rate constant could be fitted only under the assumption that the proton transfer was three orders of magnitude slower than in the WT. This model prediction is in a full agreement with the $k_{AB}^{(2)}$ independence of $\Delta G_{AB}$ in this mutant. This independence has been attributed to the slower, rate-limiting transfer of the first proton to $Q_B^-$ in the absence of Asp-L213 [54,60,67].

As we did not take into account the influence of the protonation event in the acidic cluster on the recombination kinetics when modeling the chromatophore data in Fig. 3[4], we also did not model the acidic range of the pH dependence curves in the left panel of Fig. 6. In the latter case, however, the data on the $P^+Q_B^- \rightarrow PQ_B$ recombination rate were available up to pH 5.0. It is noteworthy, that $pK_{acidic}$ values that were obtained from the fitting of the data in the right panel of Fig. 6 (see Table 6 and arrows in the left panel of Fig. 6) correlated roughly with the respective pH values at which the $P^+Q_B^- \rightarrow PQ_B$ recombination started to slow down on acidification because of a $Q_B^-$-stabilizing protonation event in the acidic cluster [7,49]. This correspondence: (1) demonstrates the intrinsic consisitency of the model; and (2) supports our suggestion on the deprotonation event in the acidic cluster as the main cause of the plateau in the pH

[4] No reliable spectrophotometric data were available at pH < 7.0; for chromatophores, the acidic segment of the pH dependence could be better resolved with the EPR technique; see ref. [49].

Table 4
The impact of amino acid substitutions on $\Delta G_{AB}$ and $pK_{212}$ in isolated RC of *Rb. sphaeroides*. See the text for details.

| Strain | $\Delta G'_{AB}$ (meV) | $\delta\Delta G'_{AB}$ (meV) | $pK_{212}$ | $\delta pK_{212}$ |
|---|---|---|---|---|
| WT | −75.9 | 0 | 9.76 | 0 |
| L213DN | −148.9 | −73.0 | 8.55 | −1.21 |
| L213DN and M44ND | −91.3 | −15.4 | 9.18 | −0.58 |
| M44ND | −30.3 | 45.6 | 10.39 | 0.62 |
| L213DN and H177RH | −43.7 | 32.2 | 8.89 | −0.88 |

dependence of the rate constant of the $Q_A^-Q_B^- \rightarrow Q_AQ_BH_2$ transition (see above).

The model yielded a $pK_1$ value for the $Q_BH^\bullet/Q_B^{\bullet-}$ couple of $\sim$4.2 in chromatophores and of $\sim$3.2 in the RC preparations (see Tables 2 and 5, respectively). The lower $pK_1$ in the RC preparations, as compared to chromatophores, is in good agreement with experimental observations of Lavergne and coworkers. They have found recently that the $Q_BH^\bullet/Q_B^{\bullet-}$ couple titrated at much lower pH values in their isolated RC preparations ($pK_1 < 4.0$) than when chromatophores in solution were studied ($pK_1 \geq 5.0$), supposedly, due to the changes in the RC environment [21].

*4.5.5. Summary*

Summarizing this section, the $Q_A^-Q_B^- \rightarrow Q_AQ_BH_2$ transition rate seems to depend both on the electrostatic potential at the $Q_B$ site and on the non-electrostatic, chemical affinity of the site to protons. Such a dual dependence elucidates why the introduction of neutral amino acid residues instead of negatively charged ones has a stronger impact on the rate of the $Q_B$ turnover, than the replacement of positively charged residues by neutral ones (see [8] for a survey of the mutation-due effects in the RC). In both cases, the disappearance of a charged residue is likely to decrease the chemical component of proton affinity. When a negatively charged residue is replaced by a neutral one, the decrease in the chemical proton affinity is *amplified* by the disappearance of a negative charge, as both impacts decrease the proton activity at the $Q_B$ site. When a positively charged residue is replaced by a neutral one, the decrease in the chemical proton affinity could be, however, fully *compensated* by the increase in the electrostatic proton affinity caused by the disappearance of a positive charge, as the example of the L217RI mutant shows. Thereby the apparently proton-repulsing, positively charged amino acid residues could *increase* the local proton activity by contributing to its chemical component (e.g. by providing water binding sites). This general conclusion relates to any enzymatic reaction. A good example in evidence is the conserved lysine residue that seems to govern the proton trapping in the cytochrome *c* oxidase [70,71]. Correspondingly, our approach, that allows to estimate separately the impact of mutations on electrostatic and chemical proton affinities by comparing the experimentally established $pK$ shifts with the structure-based electrostatic calculations, may also be applied to other enzymes.

Table 5
The final set of main parameters as calculated from the fit of experimental data in Fig. 6 (isolated RC of *Rb. sphaeroides*)

| Variable | $\gamma$ | $pK_1$ | $m_{+1}$ ($s^{-1}$) | $k_{+3}$ ($s^{-1}$, pH 7) |
|---|---|---|---|---|
| | 0.22 | 3.16 | $1.19 \cdot 10^5$ | $1.99 \cdot 10^3$ |

The same initial parameter values as in the case of chromatophores (see the top row in Table 2) were used upon the fit.

Table 6
The values of $pK_{acidic}$ and $\phi_{acidic}$ as obtained from the fit of the data in the right panel of Fig. 6 (isolated RC of *Rb. sphaeroides*)

| Strain | $pK_{acidic}$ | $\phi_{acidic}$ (mV) |
|---|---|---|
| WT | 6.10 | 106 |
| L213DN | – | – |
| L213DN and M44ND | 6.89 | 104 |
| M44ND | 5.60 | 109 |
| L213DN and H177RH | 6.85 | 73 |

### 4.6. A mechanistic model

The results of the modeling in Tables 2 and 4 show that the coupled second electron/first proton transfer reaction was faster than the binding of the second proton at room temperature ($k_{AB}^{(2)} = m_{+1} \cdot 10^{pK_1 - pH} > k_3^{app}$). Hence, the overall $Q_A^- Q_B^- \rightarrow Q_A Q_B H_2$ transition seemed to be kinetically controlled by the transfer of the second proton. The same conclusion could be drawn from the temperature dependence of the B2 rate that has been presented elsewhere [28]. Although the split of the B2 kinetic into two distinct components, $B2_{fast}$ and $B2_{slow}$, was reliably discernible only below 15°C, their extrapolation into the higher temperature range showed that $B2_{slow}$ retarded relative to $B2_{fast}$ up to ~30°C (see the Arrhenius plots in Fig. 2 of ref. [28]).

In Fig. 7, we attempted to rationalize these findings by a tentative scheme of the $Q_B$ turnover in the RC of *Rb. sphaeroides*. The scheme correlates with previously suggested mechanistic schemes of the $Q_B$ turnover in the RCs of *Rb. sphaeroides* [1] and *Rps. viridis* [72]. However, we put more emphasis on the crucial, in our opinion, alternating interaction of Glu-L212 with the $Q_B$ ring and His-L190, respectively.

As we have discussed in more detail elsewhere [19], a wealth of data on the $Q_B$ site operation in *Rb. sphaeroides* could be understood by a suggestion that the neutral ubiquinone molecule can attain two energetically comparable conformations in the binding pocket. We have hypothesized that in one conformational state the protonated form of Glu-L212 is stabilized by its interaction with the $Q_B$ ring, whereas in the other state Glu-L212 is not directly interacting with $Q_B$ and exists as a negatively charged carboxy anion at neutral pH [19]. And indeed, the cryocrystallographic studies of the *Rb. sphaeroides* RC have shown that $Q_B$ is seen in two binding sites, namely the distal and the proximal one relative to the non-heme iron and Glu-L212 [1]. In the *distal* state $Q_B^d$, ubiquinone is away from the Glu-L212. The respective structure A in Fig. 7 shows several water molecules next to Glu-L212; two of them form a bridge between Glu-L212 and His-L190 [1,72], Glu-L212 seems to serve as a hydrogen bond acceptor in such a bridge at neutral pH [72]. Based on diverse functional data, $pK_{212}$ can been estimated as ≤6.0 for the $Q_B^d$ state (see ref. [19] and references therein). In the alternative *proximal* state $Q_B^p$, the quinone ring, rotated by 180° compared to $Q_B^d$, is ~5 Å closer to Glu-L212 (see ref. [1] and structure B in Fig. 7). The presence of $Q_B^p$ prevents the formation of the water bridge between Glu-L212 and His-L190. The absence of the water bridge and the proximity of oxygen atoms of $Q_B^p$ keep Glu-L212 protonated at neutral pH. The $Q_B^p$ state seems to dominate at room temperature [19]. The $pK_{212}$ of this state corresponds to the value of ~10.0 that could be experimentally established from the pH dependence of the $P^+Q_B^- \rightarrow PQ_B$ recombination (see Section 3 and refs. [19,39,40,45] for more details).

In the fraction of the $Q_B^p$-RCs, the delivery of the first electron (B→C transition in Fig. 7) is accompanied by a minor quinone displacement into the 'semiquinone' position that has been resolved in the low-temperature structure of the light-adapted RC ([1], see structure C in Fig. 7). The $E_a$ of such a displacement is expected to be low. In the fraction of the $Q_B^d$-RC, the $Q_B^-$ formation is coupled with the movement of the quinone ring into the proximal position (A→B?→C transition in Fig. 7) accompanied by the protonation of Glu-L212 (see [1,19] for more details). As this reorganization includes the propeller twist of the quinone in the $Q_B$ pocket, the reaction is expected to be slower than in the previous case and to have a higher $E_a$. And indeed, the faster kinetic component(s) of the $Q_B$ reduction seem to be less dependent on temperature, than the slower ones. The $Q_B$ reduction has been monitored by the time-resolved IR-spectroscopy at 1487 $cm^{-1}$ ($Q_B^-$ formation) and 1725 $cm^{-1}$ (appearance of the protonated Glu-L212 [45,73]), by the UV-visible spectroscopy at 390 nm ($Q_A^-$ decay in the RC where $Q_A$ ubiquinone has been replaced by a 2-methyl-3-phytyl-1,4-naphthoquinone [16]) and at 757 nm (electrochromic response of the RC bacteriopheophytin to $Q_B^-$ formation [47]), and by electrometry via the accompanying $\Delta\psi$ changes [19]. In the case of the isolated RC preparations, the respective $E_a$ values, when estimated, were 14–16 kJ/mol for the fast component(s) and 30–40 kJ/mol for the slower one(s) [16,47]. In the case of chromatophores, the respective $E_a$ estimates were <10 and ~60 kJ/mol, respectively [19].

The further step of the $Q_B$ turnover is the joint transfer of the second electron and the first proton

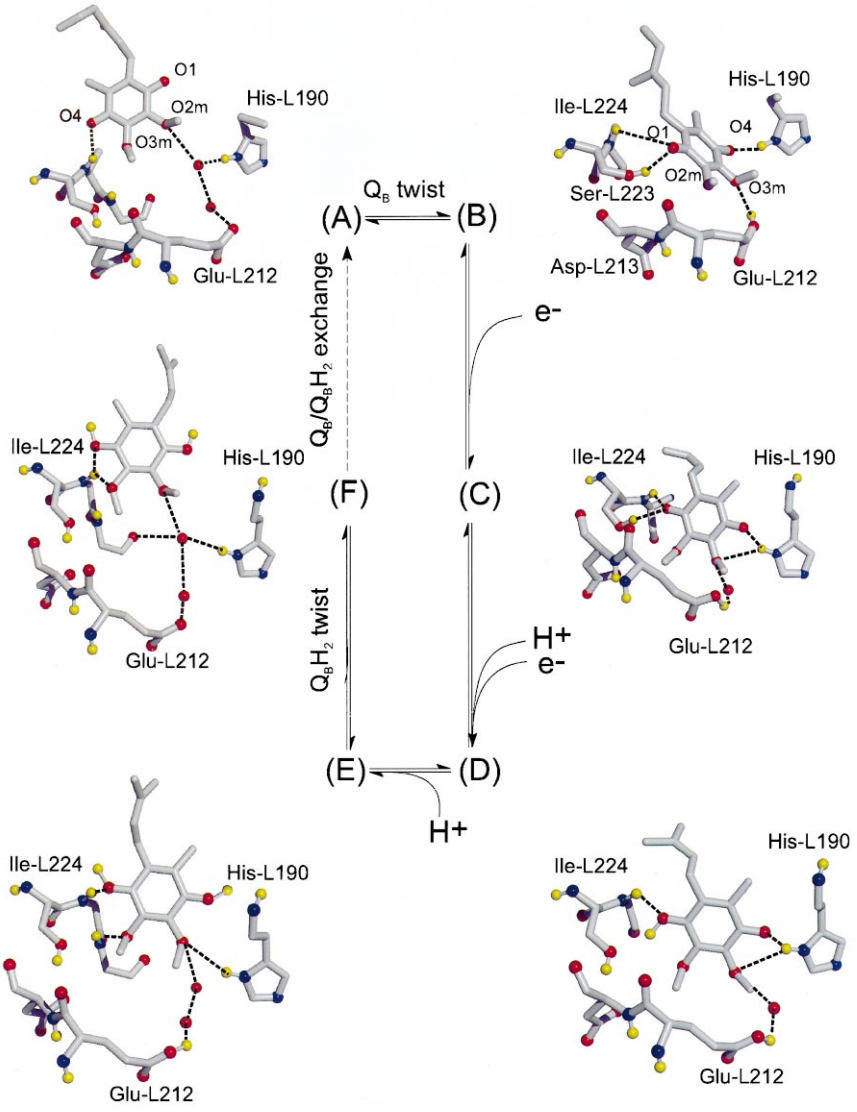


Fig. 7. The tentative scheme of the $Q_B$ turnover in the RC of *Rb. sphaeroides*. Color codes as in Fig. 1A. Hydrogen bonds are depicted by dashed lines. (A) The distal position of $Q_B$ ($Q_B^d$) as seen in the low-temperature dark-adapted RC structure (PDB entry 1AIJ [1]). (B) The proximal position of $Q_B$, $Q_B^p$ (PDB entry 2RCR, [80]). (C) The 'semiquinone' position of $Q_B^-$, as seen in the low-temperature light-adapted RC structure with a trapped $Q_B^-$ (PDB entry 1AIG [1]). $Q_B^-$ seems to be stabilized by the hydrogen bonds of carbonyl O1 with Ile-L224 and of carbonyl O4 with His-L190. Additionally, hydrogen bond-compatible distances of $\leq$3.2 Å separate Gly-L225 from the carbonyl O1 and methoxy O2 (not shown), Ser-L223 from carbonyl O1 and Thr-L226 from the methoxy O2 (not shown). (D) The position of $Q_BH^-$ is modeled after Lancaster and Michel [72] from the crystal structure of the stigmatellin-containing RC of *Rps. viridis*. Here the $O3_m$ and between Ser-L223 and the protonated O1 carbonyl. (E) The 'detached' $Q_BH_2$ is tentatively shown on its way towards the distal 'quinol' position, before the propeller twist. The hydrogen bond of carbonyl O4 with His-L190 is already broken, but the water bridge between Glu-L212 and His-L190 is not formed yet. (F) Ubiquinol $Q_BH_2$ position is modeled along the crystal structure of the RC prepared in the presence of ascorbate (PDB entry 1PCR [57]). In this structure, Ile-L224 is on a hydrogen bond distance from carbonyl O4 and methoxy $O3_m$ of the quinone ring.

to $Q_B^-$ (C→D transition in Fig. 7). The $E_a$ of this transition has been shown to be low, ~10 kJ/mol [28]. The quinone ring either does not change its position on this transition or shifts slightly to occupy a position that has been modeled from the crystal structure of the stigmatellin-containing RC of *Rps. viridis* [72] and that is shown as state D in Fig. 7. On the contrary, the higher $E_a$ of the second proton

transfer (~60 kJ/mol in chromatophores [28]) and the larger H/D ratio attributed to this reaction [74] indicate that this step could be accompanied by a structural change. As has already been discussed [28,72], the quinol ring has to twist back to attain the distal 'quinol' position in the course of ubiquinol formation. Most likely, the binding of the second proton to O4 atom of $Q_BH^-$ is *coupled* with this rotation. The high $E_a$ indicates that the detachment of the quinol ring is the rate-limiting event. Most likely, the $Q_BH^- \leftrightarrow Q_BH_2$ equilibrium is shifted to the left until $Q_BH_2$ detaches to move into the distal, *ubiquinol* position (D→E transition in Fig. 7), followed by the reset of the water bridge between Glu-L212 and His-L190 (E→F transition in Fig. 7). The water bridge is likely to prevent the reversion of the reaction and to contribute to the stabilization of $Q_BH_2$ in the distal state.

Thus, the first electron transfer is limited by the *distal to proximal* ubiquinone transition in the majority of the RC [1,19], whereas the formation of $Q_BH_2$ seems to be limited by the reverse *proximal to distal* twist of the ubiquinone ring. Therefore, $E_a$ of $B1_{slow}$ and $B2_{slow}$ (determined in [19] and [28], respectively) are comparably high. The high $E_a$ of the second protonation event makes it the rate-limiting step of the overall $Q_A^-Q_B^- \rightarrow Q_AQ_BH_2$ transition.

#### 4.6.1. *The mechanism of the $Q_B$ reduction and protonation as a whole*

Considering the mechanism of the $Q_B$ reduction and protonation as a whole, it is worthwhile to note the precise tuning of charge interactions on different steps of the RC turnover. The electro*static* calculations indicate that the surplus potential around $Q_B$ is negative [64], and as such can hardly contribute to the stabilization of $Q_B^-$. Instead, the negative charge of $Q_B^-$ is stabilized by a *dynamic* redistribution of protons in the $Q_B$ pocket after the first electron transfer [16–21,47]. Particularly the p$K_{212}$ shift from ≤6.0 in the $Q_B^d$ state to ≥12.0 in the presence of $Q_B^-$ leads to the protonation of Glu-L212 and, hence, to the appearance of a proton only 4 Å away from $Q_B^-$. Most likely, p$K_{212}$ switches back to ≤6.0 on the last step of the $Q_B$ turnover, when the formed $Q_BH_2$ detaches to move into the distal position, and the water molecules wedge in between the withdrawing quinone ring and Glu-L212 to restore the water bridge between Glu-L212 and His-L190 (compare the structures A and F in Fig. 7; see also ref. [75] for a more detailed consideration of p*K*-switching mechanism). The *negative* charge on Glu-L212 keeps the electrostatic potential in the $Q_B$ site low and prevents the deprotonation of $Q_BH_2$ until the latter exchanges for a ubiquinone from the membrane pool.

## 5. Concluding remarks

We characterized two mutants of *Rb. sphaeroides* where basic residues around $Q_B$ were replaced by the neutral ones (Arg-207→Ile and Arg-217→Ile). The decreased stability of the $Q_B^-$ state in both mutants agreed with the expected electrostatic changes at the $Q_B$ site. At the same time, more complex perturbations in the electron/proton coupling during the $Q_A^-Q_B^- \rightarrow Q_AQ_BH_2$ transition could be understood only if the mutation-caused changes in the non-electrostatic, chemical proton affinity were taken into account. We suggest that a high chemical affinity of a catalytic site to proton is as important for the attracting a proton from the bulk water, as the presence of a surplus negative charge. Based on functional studies, structural data and kinetic modeling, we suggest a mechanistic scheme of the $Q_B$ turnover. The detachment of the formed ubiquinol from its proximal position next to Glu-L212 is considered as the rate-limiting step of the reaction cycle.

## Acknowledgements

Thanks are due to Dr. Kevin Gray for the useful information concerning the site-specific mutagenesis and to Mrs. Irina Bukhova for her help in growing the photosynthetic bacteria. We wish to thank Drs. Melvin Y. Okamura and Mark L. Paddock for the access to their original experimental data prior to publication and valuable advice, and Dr. Jérôme Lavergne for the access to ref. [21] prior to publication. Drs. Andrey D. Kaulen, Lev I. Krishtalik, Roy C.D. Lancaster, Vladimir P. Shinkarev, Michael I. Verkhovsky, Colin A. Wraight and Lev S. Yaguzhin-

sky are acknowledged for valuable discussions. We thank Profs. Wolfgang Junge and Vlamidir P. Skulachev for their stimulating interest to our work. This work was supported in part by grants from the Russian Foundation for the Basic Research (99-04-48652 and 97-04-50179), the Max-Planck-Gesellschaft, the Deutsche Forschungsgemeinschaft (Mu-1285/1) and the European Commission (INTAS-93-2852).

## Appendix

Here we consider in more detail the partial reactions in Scheme III and present the mathematical solution of the corresponding kinetic model.

The first proton is, supposedly, delivered to the O1 carbonyl oxygen of $Q_B^-$ via Ser-L223 and, perhaps, Asp-L213 [8]. The acidic cluster keeps the proton activity almost constant at neutral pH, so that proton transfer is not rate-limiting [60]. For *Rb. sphaeroides* chromatophores, the rate of $B2_{fast}$ component measured at $pH_i$ of 5.7 (see Fig. 3, right panel) can be used as the lower estimate of the rate constant of the first proton delivery to $Q_B^-$. The corresponding expression for the rate constant of proton transfer would then be

$$k_{+1}, k_{+2} = 5 \cdot 10^{10-pH^*} (s^{-1}). \quad (11)$$

The second proton delivery does not limit the rate of the $Q_BH^- \rightarrow Q_BH_2$ transition, as the latter seems to be limited by the detachment of the formed ubiquinol from the proximal binding site (see the main text). Then the rate of the second proton transfer could be described by the expression

$$k_{+3} = A_3 \cdot 10^{-E_a/2.3kT} \cdot 10^{-pH^*} \quad (12)$$

where the pre-exponential factor $A_3$ is a variable parameter.

As long as the proton transfer from the surface is not rate-limiting [60], one can also define the partial equilibrium constants connected with the p$K$ values of the neutral semiquinone $Q_BH^-$ ($K_1 = 10^{pK_1-pH}$), the ubiquinol-anion $Q_BH^-$ ($K_2 = 10^{pK_2-pH}$) and the neutral ubiquinol $Q_BH_2$ ($K_3 = 10^{pK_3-pH}$). The respective p$K$ values have been estimated as $\leq 5$ for the $Q_B^{\bullet -}/Q_BH^{\bullet}$ couple (p$K_1$) [8,21,76], as $\sim 10.5$ for the $Q_B^{2-}/Q_BH^-$ (p$K_2$) couple [46], and as $\leq 9.0$ for the $Q_BH^-/Q_BH_2$ (p$K_3$) couple [46]. One could expect that at $pH > 9$, the extent of B2 would drop, because of inability of the second proton to bind at $pH > pK_3$. This was not observed. Instead, two-fold decrease of the total amplitude of electrogenic response was observed at $pH \sim 10.5$ (Fig. 5C). Apparently, the rate of the direct reaction matched the rate of the reverse one only at this pH value. Hence, the overall reaction seemed to be driven by the dissociation of ubiquinol from the site $Q_B$ at $pH > pK_3$ (see ref. [46]). The rate constant $k_{off}$ of this dissociation in chromatophores of *Rb. sphaeroides* has been estimated as $> 10^4$ $s^{-1}$ [77]. If the rate of ubiquinol release was slower than its second protonation ($k_{off} < k_{+3}$) the kinetics of B2 at $pH > 9$ should consist of two components with characteristic times corresponding to $k_{off}$ and $k_{+3}$. The apparent mono-exponentially of B2 kinetics at this pH ([17,18,28], see also Fig. 4C), indicates that the rate $k_{off}$ was faster than $k_{+3}$. Hence, the reactions determined by $k_{off}$ and $k_{on}$ could be neglected, so that we used an *apparent* p$K_3$, $pK_3^a$, that accounted both for the second protonation and ubiquinol release, throughout the modeling. We used a value of $10^3$ $s^{-1}$ as an initial estimate of $k_{+3}$, and estimated $pK_3^a$ as about 10.5 from the pH dependence of the B2 amplitude (Fig. 5C).

The rate constants of proton dissociation, $k_{-1}$, $k_{-2}$, and $k_{-3}$ could be obtained from the known rate constants of the respective direct reactions and the p$K$ values.

The equilibrium constant of the coupled transfer of the second electron and the first proton to $Q_B^-$, $M_1$, has been shown to match 1.0 at pH 8.5 with RC preparations from the L212EQ mutant [40]. In our calculations, we used an estimate that was obtained with WT chromatophores from the pH dependence of the $B2_{fast}$ amplitude in our electrometric set-up; according to it, $M_1$ matches 1.0 at pH 8.7 ([28] and unpublished observations).

$M_1$ is connected with the microscopic rate constants in a following way:

$$M_1 = \frac{k_{+1} \cdot m_{+1}}{k_{-1} \cdot m_{-1}} = \frac{k_{+2} \cdot m_{+2}}{k_{-2} \cdot m_{-2}}. \quad (13)$$

The rate constant $m_{+1}$ of the second electron delivery to $Q_BH^{\bullet}$ was estimated as $> 10^5$ $s^{-1}$ from the rate of B2 at $pH \sim 4.0$ (see Fig. 3, middle panel).

The rate constant $m_{+2}$ of the second electron

transfer to the anionic $Q_B^-$ (the bottom pathway in Scheme III) was estimated as $10^3$ $s^{-1}$ in accordance with ref. [8].

The rate constants of the reversed electron transfer reactions, $m_{-1}$ and $m_{-2}$, could be calculated from Eq. 13 by using the values of the equilibrium constants $K_1$, $K_2$ and $M_1$.

The changes in the rate of electron transfer from $Q_A^-$ to $Q_B^-$ caused by the site-specific mutations were described in the framework of the Marcus theory [61]

$$k_{AB} = \frac{\pi}{\hbar}\frac{|V|^2}{\sqrt{\pi k T \lambda}}\cdot\exp\left(-\frac{(\lambda + \Delta G^0_{AB})^2}{4\lambda k T}\right) \quad (14)$$

where $V$ is the electron matrix element and $\lambda$ is the reorganization energy. As discussed in the main text, we considered the change in the free energy difference $\delta\Delta G_{AB}$ as the main factor that influenced the electron transfer rate in the mutant chromatophores. Since in the case of electron transfer from $Q_A$ to $Q_B$, $|\Delta G_{AB}| \ll \lambda$ [78]:

$$\ln(k_{AB}) \propto -\tfrac{1}{2}\delta\Delta G_{AB}. \quad (15)$$

According to Eq. 15, the decrease of the driving force (positive $\delta\Delta G_{AB}$) slows down the direct electron transfer and accelerates the back reaction to the same extent. The rate constant $m_{\pm1}$ and $m_{\pm2}$ of the second electron transfer reactions in the mutant chromatophores have been changed according to Eq. 15 with $\delta\Delta G_{AB}$ values taken from Table 1.

## A1. Mathematical solution

To simplify the notations, it is convenient to introduce one-letter abbreviations for concentrations of different partial states of $Q_A$ and $Q_B$, respectively:

$$[Q_A^-Q_B^-] = A, [Q_A^-Q_BH^\bullet] = B, [Q_AQ_B^{2-}] = C,$$

$$[Q_AQ_BH^-] = D, [Q_AQ_BH_2] = E.$$

The system of differential equations corresponding to Scheme III could be written then as follows:

$$\begin{cases} \dot{A} = -(k_{+1} + m_{+2})\cdot A + k_{-1}\cdot B + m_{-2}\cdot C \\ \dot{B} = k_{+1}\cdot A - (k_{-1} + m_{+1})\cdot B + m_{-1}\cdot D \\ \dot{C} = m_{+2}\cdot A - (k_{+2} + m_{-2})\cdot C + k_{-2}\cdot D \\ \dot{D} = m_{+1}\cdot B + k_{+2}\cdot C - (k_{-2} + m_{-1} + k_{+3})\cdot D + k_{-3}\cdot E \\ \dot{E} = k_{+3}\cdot D - k_{-3}\cdot E \end{cases} \quad (16)$$

Because of the normalizing condition,

$$A + B + C + D + E = 1, \quad (17)$$

the real number of the differential equations is only four. Nevertheless, this system is rather complicated and should be simplified for a quantitative analysis. The reduction can be done by the standard method of stationary concentrations. According to this approximation, concentrations of the intermediate states $B$ and $C$ are treated as being in fast equilibrium with the slowly changing variables $A$, $D$, and $E$. This conclusion directly follows from the fact that concentrations of the states $B$ and $C$ are always small due to the low p$K$ value of semiquinone $Q_BH^\bullet$ and the low redox potential of quinol-dianion $Q_B^{2-}$, respectively (see, for example, [8]). Applying the evident relationships between the rate constants

$$k_{-1} + m_{+1} \gg k_{+1}, m_{-1} \text{ and } k_{+2} + m_{-2} \gg k_{-2}, m_{+2}$$

one can obtain the expressions for the stationary concentrations of the intermediate states:

$$B = \frac{k_{+1}\cdot A + m_{-1}\cdot D}{k_{-1} + m_{+1}},\ C = \frac{m_{+2}\cdot A + k_{-2}\cdot D}{k_{+2} + m_{-2}}. \quad (18)$$

Together with the normalizing Eq. 17, this leads to a significant simplification of the system (Eq. 16). The final system includes only two linear differential equations

$$\begin{cases} \dot{D} = c_{11}\cdot D + c_{12}\cdot E + c_1 \\ \dot{E} = c_{21}\cdot D + c_{22}\cdot E + c_2 \end{cases} \quad (19)$$

with the linear coefficients being defined as follows:

$$c_{11} = -\left[\frac{k_{+1}m_{+1}}{k_{-1}+m_{+1}} + \frac{k_{+2}m_{+2}}{k_{+2}+m_{-2}}\right]\cdot\frac{(k_{-1}+m_{+1})\cdot(k_{+2}+m_{-2}) + m_{-1}(k_{+2}+m_{-2}) + k_{-2}(k_{-1}+m_{+1})}{(k_{-1}+m_{+1})\cdot(k_{+2}+m_{-2}) + k_{+1}(k_{+2}+m_{-2}) + m_{+2}(k_{-1}+m_{+1})} + \frac{m_{+1}m_{-1}}{k_{-1}+m_{+1}} + \frac{k_{+2}k_{-2}}{k_{+2}+m_{-2}} - k_{-2} - m_{-1} - k_{+3}$$

$$c_{12} = k_{-3} - \frac{k_{+1}m_{+1}\cdot(k_{+2}+m_{-2}) + k_{+2}m_{+2}(k_{-1}+m_{+1})}{(k_{-1}+m_{+1})\cdot(k_{+2}+m_{-2}) + k_{+1}(k_{+2}+m_{-2}) + m_{+2}(k_{-1}+m_{+1})}$$

$$c_1 = \frac{k_{+1}m_{+1}\cdot(k_{+2}+m_{-2}) + k_{+2}m_{+2}(k_{-1}+m_{+1})}{(k_{-1}+m_{+1})\cdot(k_{+2}+m_{-2}) + k_{+1}(k_{+2}+m_{-2}) + m_{+2}(k_{-1}+m_{+1})}$$

$$c_{21} = k_{+3}$$

$$c_{22} = k_{-3}$$

$$c_2 = 0.$$

The system (Eq. 19) has a two-exponential general solution:

$$\begin{aligned} D(t) &= D_0 + D_1\cdot\exp(-\lambda_1 t) + D_2\cdot\exp(-\lambda_2 t) \\ E(t) &= E_0 + E_1\cdot\exp(-\lambda_1 t) + E_2\cdot\exp(-\lambda_2 t) \end{aligned} \quad (20)$$

with the characteristic roots $\lambda_1$ and $\lambda_2$ defined by the equation

$$\lambda_{1,2} = -\frac{1}{2}\left(c_{11} + c_{22} \mp \sqrt{(c_{11}-c_{22})^2 + 4c_{12}c_{12}}\right).$$

## A2. Kinetic model for Rb. sphaeroides chromatophores

At pH below 8.7 ($M_1 > 1$), the reaction of the coupled second electron/first proton transfer is independent of the binding of the second proton. Consequently, the $B2_{fast}$ and $B2_{slow}$ components, that are observable at low temperatures [28], could be directly assigned to the two exponents of Eq. 20. The relative amplitudes of two components approximately matched each other [28] so we could define the average rate of the phase B2 as $k = 0.5\cdot(\lambda_1+\lambda_2)$.

At pH > 8.7 ($M_1 < 1$), the driving force behind the whole process is the binding of a second proton to $Q_B$, followed by the fast dissociation of a ubiquinol from the site $Q_B$. Under these conditions, the electrogenic phase B2 is expected to be intrinsically monoexponential, in line with experimental evidence [28]. Hence, the rate of the phase B2 could be written as $k = \lambda_2$.

The rate of the $Q_A^- Q_B^- \rightarrow Q_A Q_B H_2$ reaction in the whole pH interval could then be approximated by the equation:

$$k = \frac{\lambda_2 + 0.5\cdot(\lambda_1+\lambda_2)\cdot M_1}{1+M_1}. \quad (21)$$

## A3. Kinetic model for the isolated RC

With RC preparations (Fig. 6 and Tables 3–5), where the pH dependence of the rate constant of the second electron transfer, $k_{AB}^{(2)}$, but not of B2 were available, we used another mono-exponential approximation to model the $Q_A^- Q_B^- \rightarrow Q_A Q_B H^-$ transition (cf. Eq. 21):

$$k = \frac{\lambda_2 + \lambda_1\cdot M_1}{1+M_1} \quad (22)$$

In this case, the kinetics of electron transfer were approximated by the fast component at pH < 8.7 and by the slow component at pH > 8.7, respectively. We used this equation for the WT and mutant RCs, except the L213DN. In the latter case, the slow transfer of protons seems to control the reaction, and we approximated the kinetics of electron transfer by the slow component at all pH values. For simplicity, we neglected the lower kinetic path in Scheme III during the RC calculations, as evidence against involvement of this reaction route in the case of the isolated RC has been presented [60,67].

## References


[1] M.H. Stowell, T.M. McPhillips, D.C. Rees, S.M. Soltis, E. Abresch, G. Feher, Science 276 (1997) 812–816.
[2] G. Fritzsch, L. Kampmann, G. Kapaun, H. Michel, Photosynth. Res. 55 (1998) 127–132.
[3] C.R.D. Lancaster, H. Michel, Photosynth. Res. 48 (1996) 65–74.
[4] W.W. Parson, in: H. Scheer (Ed.), Chlorophylls, CRC Press, Boca Raton, FL, 1991, pp. 1153–1180.
[5] M.Y. Okamura, G. Feher, Annu. Rev. Biochem. 61 (1992) 861–896.
[6] P. Maroti, Photosynth. Res. 31 (1993) 1–17.
[7] V.P. Shinkarev, C.A. Wraight, in: J. Deisenhofer, J.R. Norris (Eds.), The Photosynthetic Reaction Center, Vol. 1, Academic Press, San Diego, 1993, pp. 193–255.
[8] M.Y. Okamura, G. Feher, in: R.E. Blankenship, M.T. Madigan, C.E. Bauer (Eds.), Anoxygenic Photosynthetic Bacteria, Kluwer Academic, Doordrecht, 1995, pp. 577–594.
[9] P. Sebban, P. Maroti, D.K. Hanson, Biochimie 77 (1995) 677–694.
[10] A.Y. Mulkidjanyan, V.P. Shinkarev, M.I. Verkhovsky, B.S. Kaurov, Biochim. Biophys. Acta 849 (1986) 150–161.
[11] P.H. McPherson, M.Y. Okamura, G. Feher, Biochim. Biophys. Acta 1016 (1990) 289–292.
[12] C.A. Wraight, Biochim. Biophys. Acta 548 (1979) 309–327.
[13] P. Maroti, C.A. Wraight, Biochim. Biophys. Acta 934 (1988) 329–347.
[14] P.H. McPherson, M.Y. Okamura, G. Feher, Biochim. Biophys. Acta 934 (1988) 348–368.
[15] O.A. Gopta, D.A. Cherepanov, W. Junge, A.Y. Mulkidjanian, Proc. Natl. Acad. Sci. USA 96 (1999) 13159–13164.
[16] J. Li, D. Gilroy, D.M. Tiede, M.R. Gunner, Biochemistry 37 (1998) 2818–2829.
[17] L.A. Drachev, M.D. Mamedov, A.Y. Mulkidjanian, A.Y. Semenov, V.P. Shinkarev, M.I. Verkhovsky, FEBS Lett. 259 (1990) 324–326.
[18] M.I. Verkhovskii, L.A. Drachev, M.D. Mamedov, A.Y. Mulkidzhanyan, A.Y. Semenov, V.P. Shinkarev, Biokhimiya 55 (1990) 387–394.
[19] O.A. Gopta, D.A. Bloch, D.A. Cherepanov, A.Y. Mulkidjanian, FEBS Lett. 412 (1997) 490–494.
[20] P. Brzezinski, M.L. Paddock, M.Y. Okamura, G. Feher, Biochim. Biophys. Acta 1321 (1997) 149–156.
[21] J. Lavergne, C. Mattews, N. Ginet, Biochemistry 38 (1999) 4542–4552.
[22] P.H. McPherson, M.Y. Okamura, G. Feher, Biochim. Biophys. Acta 1144 (1993) 309–324.
[23] P. Maroti, J. Photochem. Photobiol. 8 (3) (1991) 263–277.
[24] J.R. Bowyer, G.V. Tierney, A.R. Crofts, FEBS Lett. 101 (1979) 201–206.
[25] A. Vermeglio, in: B.L. Trumpower (Ed.), Function of Quinones in Energy Conserving Systems, 1982, pp. 169–180.
[26] G. Feher, M.y. Okamura, in: C. Sybesma (Ed.), Advances in Photosynthesis Research: Proceedings of the VIth International Congress on Photosynthesis, Nijhoff/Junk, The Hague, 1984, pp. 155–164.
[27] O.P. Kaminskaya, A.L. Drachev, A.A. Konstantinov, A.Y. Semenov, V.P. Skulachev, FEBS Lett. 202 (1986) 224–228.
[28] O.A. Gopta, D.A. Cherepanov, A.Y. Semenov, A.Y. Mulkidjanian, D.A. Bloch, Photosynth. Res. 55 (1998) 309–316.
[29] J.W. Farchaus, D. Oesterhelt, EMBO J. 8 (1989) 47–54.
[30] K. Friedrich, H. Kolmar, H.J. Fritz, Nucleic Acids Res. 17 (1989) 5862.
[31] P. Stanssen, C. Opsomer, Y.M. McKeown, W. Kramer, M. Zabeau, H.J. Fritz, Nucleic Acids Res. 17 (1989) 4441–4454.
[32] G. Ditta, T. Schmidkauser, E. Yakobson, P. Lu, X. Liang, D.R. Finlay, D. Guiney, D.R. Helinski, Plasmid 13 (1985) 149–153.
[33] J. Davis, T.J. Donohue, S. Kaplan, J. Bacteriol. 170 (1988) 320–329.
[34] J.W. Farchaus, H. Gruenberg, D. Oesterhelt, J. Bacteriol. 172 (1990) 977–985.
[35] L.A. Drachev, A.D. Kaulen, L.V. Khitrina, V.P. Skulachev, Eur. J. Biochem. 117 (1981) 461–470.
[36] S.W. Provencher, Biophys. J. 16 (1976) 27–41.
[37] M.J.D. Powell, in: J.B. Rosen, O.L. Mangasarian, K. Ritter (Eds.), Nonlinear Programming, Academic Press, London, 1970, pp. 31–65.
[38] S.K. Chamorovsky, S.M. Remennikov, A.A. Kononenko, P.S. Venediktov, A.B. Rubin, Biochim. Biophys. Acta 430 (1976) 62–70.
[39] M.L. Paddock, S.H. Rongey, G. Feher, M.Y. Okamura, Proc. Natl. Acad. Sci. USA 86 (1989) 6602–6606.
[40] E. Takahashi, C.A. Wraight, Biochemistry 31 (1992) 855–866.
[41] V.P. Shinkarev, L.A. Drachev, M.D. Mamedov, A.J. Mulkidjanian, A.Y. Semenov, M.I. Verkhovsky, Biochim. Biophys. Acta 114 (1993) 285–294.
[42] L.A. Drachev, A.Y. Semenov, V.P. Skulachev, I.A. Smirnova, S.K. Chamorovsky, A.A. Kononenko, A.B. Rubin, N.Y. Uspenskaya, Eur. J. Biochem. 117 (1981) 483–489.
[43] S.K. Chamorovsky, A.L. Drachev, L.A. Drachev, A.K. Karagul'yan, A.A. Kononenko, A.B. Rubin, A.Y. Semenov, V.P. Skulachev, Biochim. Biophys. Acta 808 (1985) 201–208.
[44] K.M. Giangiacomo, D.E. Robertson, M.R. Gunner, P.L. Dutton, in: J. Biggins (Ed.), Progress in Photosynthetic Research, Vol. II, Nijhoff/Junk, Dordrecht, The Hague, 1987, pp. 409–412.
[45] R. Hienerwadel, S. Gryzbek, C. Fogel, W. Kreutz, M.Y. Okamura, M.L. Paddock, J. Breton, E. Nabedryk, W. Mantele, Biochemistry 34 (1995) 2832–2843.
[46] P.H. McPherson, M. Schoenfeld, M.L. Paddock, M.Y. Okamura, G. Feher, Biochemistry 33 (1994) 1181–1193.
[47] D.M. Tiede, J. Vazquez, J. Cordova, P.A. Marone, Biochemistry 35 (1996) 10763–10775.
[48] D.M. Tiede, L. Utschig, D.K. Hanson, D.M. Gallo, Photosynth. Res. 55 (1998) 267–273.
[49] V.D. Sled', V.P. Shinkarev, M.I. Verkhovsky, P.T. Mominov, V.N. Verkhoturov, K.N. Timofeev, B.S. Kaurov, Biol. Membr. Moscow 2 (1985) 1016–1022.

[50] L. Baciou, I. Sinning, P. Sebban, Biochemistry 30 (1991) 9110–9116.
[51] V.P. Shinkarev, E. Takahashi, C.A. Wraight, in: J. Breton, A. Vermeglio (Eds.), The Photosynthetic Bacterial Reaction Center II, Plenum Press, New York, 1992, pp. 375–387.
[52] E. Takahashi, P. Maroti, C.A. Wraight, in: A. Müller, E. Diemann, W. Junge, H. Ratajczak (Eds.), Electron and Proton Transfer in Chemistry and Biology, Elsevier, Amsterdam, 1992, pp. 219–236.
[53] P. Maroti, D.K. Hanson, L. Baciou, M. Schiffer, P. Sebban, Proc. Natl. Acad. Sci. USA 91 (1994) 5617–5621.
[54] M.L. Paddock, G. Feher, M.Y. Okamura, Biochemistry 36 (1997) 14238–14249.
[55] P. Maroti, D.K. Hanson, M. Schiffer, P. Sebban, Nat. Struct. Biol. 2 (1995) 1057–1059.
[56] P. Beroza, D.R. Fredkin, M.Y. Okamura, G. Feher, in: J. Breton, A. Vermeglio (Eds.), The Photosynthetic Bacterial Reaction Center II, Plenum Press, New York, 1992, pp. 363–374.
[57] U. Ermler, G. Fritzsch, S.K. Buchanan, H. Michel, Structure 2 (1994) 925–936.
[58] E.C. Abresch, M.L. Paddock, M.B. Stowell, T.M. McPhillips, H.L. Axelrod, S.M. Soltis, D.C. Rees, M.Y. Okamura, G. Feher, Photosynth. Res. 55 (1998) 119–125.
[59] M.S. Graige, G. Feher, M.Y. Okamura, Proc. Natl. Acad. Sci. USA 95 (1998) 11679–11684.
[60] M.S. Graige, M.L. Paddock, J.M. Bruce, G. Feher, M.Y. Okamura, J. Am. Chem. Soc. 118 (1996) 9005–9016.
[61] R.A. Marcus, N. Sutin, Biochim. Biophys. Acta 811 (1985) 265–322.
[62] A.Y. Semenov, M.D. Mamedov, V.P. Shinkarev, M.I. Verkhovsky, N.I. Zakharova, in: G. Drews, E.A. Dawes (Eds.), Molecular Biology of Membrane-Bound Complexes in Phototrophic Bacteria, Plenum Press, New York, 1990, pp. 329–335.
[63] M.R. Gunner, B. Honig, in: J. Breton, A. Vermeglio (Eds.), The Photosynthetic Bacterial Reaction Center II, Plenum Press, New York, 1992, pp. 403–410.
[64] P. Beroza, D.R. Fredkin, M.Y. Okamura, G. Feher, Biophys. J. 68 (1995) 2233–2250.
[65] M.L. Paddock, S.H. Rongey, P.H. McPherson, A. Juth, G. Feher, M.Y. Okamura, Biochemistry 33 (1994) 734–745.
[66] A.J. Chirino, E.J. Lous, M. Huber, J.P. Allen, C.C. Schenck, M.L. Paddock, G. Feher, D.C. Rees, Biochemistry 33 (1994) 4584–4593.
[67] M.L. Paddock, M.E. Senft, M.S. Graige, S.H. Rongey, T. Turanchik, G. Feher, M.Y. Okamura, Photosynth. Res. 55 (1998) 281–291.
[68] C.R.D. Lancaster, H. Michel, B. Honig, M.R. Gunner, Biophys. J. 70 (1996) 2469–2492.
[69] S.H. Rongey, M.L. Paddock, G. Feher, M.Y. Okamura, Proc. Natl. Acad. Sci. USA 90 (1993) 1325–1329.
[70] T.V. Vygodina, C. Pecoraro, D. Mitchell, R. Gennis, A.A. Konstantinov, Biochemistry 37 (1998) 3053–3061.
[71] P. Adelroth, R.B. Gennis, P. Brzezinski, Biochemistry 37 (1998) 2470–2476.
[72] C.R.D. Lancaster, H. Michel, Structure 5 (1997) 1339–1359.
[73] R. Hienerwadel, S. Grzybek, M. Paddock, M. Okamura, W. Mäntele, in: J. Breton, E. Nabedryk, A. Vermeglio (Eds.), Reaction Centers of Photosynthetic Purple Bacteria: Structure, Spectroscopy, Dynamics (Proceedings of the Conference), CEA, Direction des Sciences du Vivant, Cadarache, France, 1997.
[74] A. Naucler, P. Brzezinski, in: Abstracts of 11th International Biophysics Congress, Budapest, Hungary, 1993, p. 183.
[75] A.Y. Mulkidjanian, FEBS Lett. 463 (1999) 199–204.
[76] C.A. Wraight, Biochim. Biophys. Acta 459 (1977) 525–531.
[77] A.Y. Mulkidjanian, M.D. Mamedov, A.Y. Semenov, V.P. Shinkarev, M.I. Verkhovsky, L.A. Drachev, FEBS Lett. 277 (1990) 127–130.
[78] K.M. Giangiacomo, P.L. Dutton, Proc. Natl. Acad. Sci. USA 86 (1989) 2658–2662.
[79] M.L. Connolly, J. Mol. Graph. 4 (1986) 93–96.
[80] C.H. Chang, O. El-Kabbani, D. Tiede, J. Norris, M. Schiffer, Biochemistry 30 (1991) 5352–5360.
[81] A. Miller, D. Oesterhelt, Biochim. Biophys. Acta 120 (1990) 57–64.